

VETTING GALACTIC LEAVITT LAW CALIBRATORS USING RADIAL VELOCITIES:
ON THE VARIABILITY, BINARITY, AND POSSIBLE PARALLAX ERROR OF 19 LONG-PERIOD CEPHEIDS

R. I. ANDERSON^{1,2}, S. CASERTANO³, A. G. RIESS^{1,3}, C. MELIS⁴,
B. HOLL⁵, T. SEMAAN⁵, P. I. PAPICS⁶, S. BLANCO-CUARESMA⁵, L. EYER⁵, N. MOWLAVI⁵, L. PALAVERSA⁵, M. ROELEN⁵

¹Department of Physics and Astronomy, The Johns Hopkins University, 3400 N Charles St, Baltimore, MD 21218, USA

²Swiss National Science Foundation Fellow

³Space Telescope Science Institute, 3700 San Martin Dr, Baltimore, MD 21218, USA

⁴Center for Astrophysics and Space Sciences, University of California, San Diego, CA 92093, USA

⁵Département d'Astronomie, Université de Genève, 51 Ch. des Maillettes, 1290 Sauverny, Switzerland

⁶Instituut voor Sterrenkunde, KU Leuven, Celestijnenlaan 200D, B-3001 Leuven, Belgium

ABSTRACT

We investigate the radial velocity (RV) variability and spectroscopic binarity of 19 Galactic long-period ($P_{\text{puls}} \gtrsim 10$ d) classical Cepheid variable stars whose trigonometric parallaxes are being measured using the *Hubble* Space Telescope and *Gaia*. Our primary objective is to constrain possible parallax error due to undetected orbital motion. Using > 1600 high-precision RVs measured between 2011 and 2016, we find no indication of orbital motion on $\lesssim 5$ yr timescales for 18 Cepheids and determine upper limits on allowed configurations for a range of input orbital periods. The results constrain the unsigned parallax error due to orbital motion to $< 2\%$ for 16 stars, and $< 4\%$ for 18. We improve the orbital solution of the known binary YZ Carinae and show that the astrometric model must take into account orbital motion to avoid significant error ($\sim \pm 100 \mu\text{arcsec}$). We further investigate long-timescale ($P_{\text{orb}} > 10$ yr) variations in pulsation-averaged velocity v_γ via a template fitting approach using both new and literature RVs. We discover the spectroscopic binarity of XZ Car and CD Cyg, find first tentative evidence for AQ Car, and reveal KN Cen's orbital signature. Further (mostly tentative) evidence of time-variable v_γ is found for SS CMa, VY Car, SZ Cyg, and XPup. We briefly discuss considerations regarding a vetting process of Galactic Leavitt law calibrators and show that light contributions by companions are insignificant for most distance scale applications.

Keywords: binaries: general, binaries: spectroscopic, stars: distances, stars: variables: Cepheids

1. INTRODUCTION

The Cepheid¹ period-luminosity relation (PLR, [Leavitt & Pickering 1912](#), also referred to as Leavitt law) has been a crucial tool for determining extragalactic distances for more than a century ([Hertzsprung 1913](#)). Thanks to space-based astrometric measurements made by the *Hipparcos* satellite ([Perryman & ESA 1997](#); [van Leeuwen 2007](#)) and the *Hubble* Space Telescope (*HST*) ([Benedict et al. 2002](#)), this calibration has been established using absolute magnitudes estimated based on trigonometric parallax (e.g. [Feast & Catchpole 1997](#); [Benedict et al. 2007](#); [van Leeuwen et al. 2007](#)). These Cepheid parallax measurements have greatly contributed to the overall increase in accuracy of the deter-

mination of the local value of the Hubble constant H_0 ([Freedman et al. 2001](#); [Riess et al. 2009, 2011](#)), which has recently been measured to within 2.4% accuracy ([Riess et al. 2016](#)). Further extensive efforts are under way to reduce this uncertainty to 1% in order to improve the ability to interpret the Cosmic Microwave Background measured using *PLANCK* and *WMAP* and learn about the nature of Dark Energy (see discussions in e.g. [Suyu et al. 2012](#); [Weinberg et al. 2013](#)).

Parallax measurements are the “gold standard” of distance measurement, since the technique is insensitive to the intricacies of stellar physics. The ongoing ESA space mission *Gaia* is currently measuring the positions, proper motions, and parallaxes of 1 billion stars in the Galaxy, among which will be thousands of Cepheids ([Eyer et al. 2012](#), and references therein), a couple hundreds of which are expected to have parallax determined to better than 3%. In the meantime, [Riess et al. \(2014\)](#) have developed a new method of determining parallax

ria@jhu.edu

¹ We here use the term Cepheid to denote classical type-I Cepheids whose prototype is δ Cephei

by spatially scanning *HST/WFC3*. The *SHOES* team is now applying this new technique to 19 long-period ($P_{\text{puls}} \gtrsim 10$ d) Galactic Cepheids, which are particularly important for extragalactic applications of the Leavitt law, and has recently been shown to yield the intended accuracy of $\sim 20\text{--}40\mu\text{arcsec}$ (Casertano et al. 2016). *HST/WFC3* spatial scan parallaxes provide an important complement to *Gaia* parallaxes due to different systematic uncertainties involved in narrow and wide-angle astrometry. Moreover, the *HST/WFC3* parallax measurements are expected to be available before the final *Gaia* data release and can anchor a new determination of H_0 .

The imminent era of highly accurate parallaxes for hundreds of Cepheids will enable an improved sample selection for the calibration of the Cepheid Leavitt law. In analogy to selections made on the sample of type Ia supernovae, subsets of Cepheids may be selected for PLR calibration depending on properties besides fractional parallax uncertainty. Some sample selection criteria seem obvious, for instance that objects with low reddening are preferred or that long-period Cepheids are better analogues for extragalactic work due to their higher luminosities. Another potentially important point is binarity, which has been frequently mentioned in the literature as representing a difficulty for PLR calibration. A more complete list of considerations should include differences in the selection and measurement process among Galactic and extragalactic Cepheids, such as the impact of photometric zero-points, which is crucial for reducing covariance among the various rungs of the distance ladder (Riess et al. 2016). Possible differences in selection procedures include binarity and outlier rejection.

While Galactic Cepheids may be scrutinized for binarity, obtaining the same information for extragalactic Cepheids does not currently seem feasible. Similarly, Galactic Cepheids offer the opportunity to study Cepheid variability in greater detail than extragalactic Cepheids. Historically, the concept of stellar populations introduced by Baade (1944) eventually resulted in the understanding that type-II and type-I Cepheids follow different PLRs and had a tremendous impact on the understanding of the size and age of the universe (for a discussion, see Baade 1956). More subtle differences may yet exist among the objects now classified as type-I Cepheids, and detailed studies of Galactic members of this class will be essential for investigating this possibility.

Taking a first step towards clarifying the role of binarity on PLR calibration, we here present a detailed investigation of *spectroscopic* binarity of the 19 Cepheids for which *HST/WFC3* spatial scan parallaxes are being recorded. The primary aims of this investigation are to

take stock of the spectroscopic binarity of the program stars, as well as to set upper limits on undetected companions and the potential parallax error resulting from modeling the *HST* astrometric data of a binary Cepheid as a single star. We further provide a detailed description of the morphology of the radial velocity (RV) variability of the program Cepheids, report the average velocities, and briefly consider the potential for unresolved companions stars to affect Cepheid luminosity estimation.

This paper is structured as follows. §2.1 presents the initial selection of the program stars. The following §2.2 describes more than 1600 high-precision RV observations obtained using three telescopes and spectrographs. §3.1 describes the modeling of RV curves for pulsation and orbital motion. §3.2 presents the pulsational variability of the program Cepheids. §3.3 discusses caveats involved in such modeling of high-precision Cepheid RV data. §4 presents the results obtained related to spectroscopic binarity. In §4.1 we determine upper limits on undetected RV orbital motion over the baseline of our observations ($P_{\text{orb}} \lesssim 5$ yr) and use these results to constrain possible parallax error due to orbital motion for 18 of the 19 program Cepheids. §4.2 presents an improved orbital solution for YZ Carinae as well as an estimation of this orbit’s influence on the parallax measurement. Longer-timescale ($P_{\text{orb}} > 10$ yr) spectroscopic binarity is investigated in §4.3, which is divided into subsections for newly-reported candidates (§4.3.1) and ones previously discussed in the literature (§4.3.2). Additional considerations pertaining to the (general) binarity and variability of Cepheids in the context of distance measurements are provided in §5. The final §6 summarizes all results.

2. OBSERVATIONS & DATA

2.1. Sample selection

The Cepheid sample investigated here was selected according to several criteria. As the primary goal is to determine parallax accurately using *HST/WFC3* spatial scans (see Riess et al. 2014; Casertano et al. 2016), the most crucial selection criteria were ones centered on the astrometric measurement itself.

An optimal target for high-accuracy spatial scan parallax measurements has

- pulsation period longer than approximately 10 days as this reflects the periods of the predominant group of Cepheids found in other galaxies (due to higher luminosity) (S. L. Hoffmann et al., submitted) and avoids putative non-linearities of the PLR intervening at 10 d (for differing recent opinions on the matter, see Inno et al. 2013; Bhardwaj et al. 2016; García-Varela et al. 2016)
- mean V -band magnitude fainter than 7.5 to avoid

saturation (H -band > 5 mag).

- at least 5, ideally more than 10, reference stars within 6 magnitudes of the Cepheid for which trails would be recorded simultaneously.
- an expected distance of $d \lesssim 3$ kpc so that parallax can be determined to better than 10% for each individual Cepheid for a nominal parallax uncertainty of 20–40 μ arcsec.
- no known companion star with P_{orb} on the order of the sparsely-sampled *HST/WFC3* spatial scan observations (typically 5 epochs).
- extinction ($A_H \lesssim 0.5$ mag) to avoid excessive uncertainty in the inferred absolute magnitudes.

Although binaries were not strictly excluded from the sample (see, e.g., YZ Carinae below or visual binaries), we caution that the present sample is subject to selection effects concerning binarity and should not be considered random in this regard. Therefore, we stress that this sample alone should not be used to infer the properties of binary fractions unless this occurs in conjunction with further observational data capable of eliminating or reducing such selection effects (Evans et al. 2013).

2.2. Description of observations

We have secured time-series observations from three different high-resolution echelle spectrographs: *Coralie* ($R \sim 60,000$) at the Swiss 1.2 m Euler telescope located at La Silla Observatory, Chile; *Hermes* ($R \sim 85,000$) at the Flemish 1.2 m Mercator telescope² located at the Roque de los Muchachos Observatory on La Palma, Canary Islands, Spain; *Hamilton* ($R \sim 60,000$) at the 3 m Shane telescope located at Lick Observatory, California, USA.

Coralie and *Hermes* spectra were reduced using the dedicated pipelines available on site. *Hamilton* spectra were reduced using standard IRAF routines. All spectra were bias-corrected and flat-fielded, and cosmic ray hits were removed. ThAr (*Coralie*, *Hermes*) and TiAr (Pakhomov & Zhao 2013, *Hamilton*) lamps were used for wavelength calibration.

All radial velocities (RVs) presented here were determined using the cross-correlation technique (Baranne et al. 1996; Pepe et al. 2002) using a numerical mask representative of a solar spectral type (G2 mask).

Coralie RVs were corrected for temporal variations in the wavelength calibration using ThAr reference spectra that are interlaced with the science orders on the detector. *Hermes* spectra were corrected for such variations

using frequent re-calibration of the wavelength solution and a model for estimating RV zero-point changes associated with changes in air pressure (as done in Anderson et al. 2015). *Hamilton* spectra are the most affected by temporal variations in the instrumental zero-point, which dominate the uncertainty for the associated RVs presented here. We use stable RV standard stars to track the RV variation due to intra-night changes of the wavelength solution and determine appropriate corrections for science exposures by interpolating the time sequence of offsets determined.

The precision of *Coralie* and *Hermes* measurements is typically on the order of 10–30 ms^{-1} , depending on the signal-to-noise ratio (SNR) achieved. At this level of precision, the instrumental zero-points of *Coralie* and *Hermes* are compatible without adjustments. *Hamilton* RVs are significantly less precise due to the unstable zero-point; here we adopt 200 ms^{-1} as a typical uncertainty for *Hamilton* RVs. This value includes the uncertainty associated with tracking the nightly zero-point variations using standard stars as well as (smaller) RV zero-point differences among instruments.

The time of observation for all newly-observed spectra are given as solar system barycentric Julian dates minus 2 400 000 and all associated RV measurements are relative to the solar system barycenter.

3. RADIAL VELOCITY MODELING

3.1. Methodology

The observed RV curve of a (binary) Cepheid is a superposition of the systemic RV relative to the Solar system barycenter, v_γ , the pulsational variability, $v_{r,\text{puls}}$, and the orbital motion of the Cepheid relative to the center of gravity of the binary system, $v_{r,\text{orb}}$. Thus,

$$v_r(t) = v_\gamma + v_{r,\text{puls}} + v_{r,\text{orb}}. \quad (1)$$

We model the pulsational variability as a Fourier series with an appropriate (fixed) number of harmonics, N_{FS} , which is adopted during a preliminary inspection of the available RV data, cf. Tab. 3. The Fourier model of the pulsation is computed as:

$$v_{r,\text{puls}}(t) = \sum_{i=1}^N a_i \sin 2\pi\phi_{\text{puls}} + b_i \cos 2\pi\phi_{\text{puls}}, \quad (2)$$

with pulsation phase $\phi_{\text{puls}} = (t - E)/P_{\text{puls}}$, where t is time in Julian days, E is the reference epoch, and P_{puls} is determined by minimizing the internal scatter of our RV data using as starting point a reference value from the General Catalog of Variable Stars (Samus et al. 2009). We here employ a definition of the epoch E so that $\phi = 0.0$ coincides with minimal RV near the mean (solar system) barycentric JD of the data considered. This choice of phase zero-point is arbitrary and not of

² <http://www.mercator.iac.es/>

Table 1. Basic information on the sample of Cepheids discussed here

Cepheid	HD	RA(J2000) [h:m:s]	DE(J2000) [d:m:s]	$\langle m_V \rangle$ [mag]	N_{Cor}	N_{Ham}	N_{Her}	Δt_{obs} [yr]	References
SY Aur	277622	05:12:39.20	42:49:54	9.1	0	78	31	2.6	–
SS CMa	HIP 36088	07:26:07.20	-25:15:26	9.9	24	42	14	3.0	1, 2, 3
VY Car	93203	10:44:32.70	-57:33:55	7.5	83	0	0	5.0	1, 2, 4, 5, 6
XY Car	308149	11:02:16.10	-64:15:46	9.3	70	0	0	1.9	–
XZ Car	305996	11:04:13.50	-60:58:48	8.6	118	0	0	4.2	§4.3.1
YZ Car	90912	10:28:16.80	-59:21:01	8.7	28	0	0	2.4	7, 8, §4.2
AQ Car	89991	10:21:23.00	-61:04:27	8.9	59	0	0	1.9	§4.3.1
HW Car	92490	10:39:20.30	-61:09:09	9.2	68	0	0	5.0	–
DD Cas	HIP 118122	23:57:35.00	62:43:06	9.9	0	78	23	2.3	9, 10
KN Cen	HIP 66383	13:36:36.90	-64:33:30	9.9	70	0	0	2.1	9, 11, 12, 13, 14, 15
SZ Cyg	196018	20:32:54.30	46:36:05	9.4	0	66	41	2.3	16, 17, §4.3.1
CD Cyg	227463	20:04:26.60	34:06:44	9.0	0	66	45	2.3	§4.3.1
VX Per	236948	02:07:48.50	58:26:37	9.4	0	78	40	4.0	–
X Pup	60266	07:32:47.00	-20:54:35	8.6	48	21	15	1.4	18
AQ Pup	65589	07:58:22.10	-29:07:48	8.7	51	41	6	3.0	10, 19, 20
WZ Sgr	167660	18:16:59.70	-19:04:33	8.1	48	6	29	4.0	5, 15, 21, 22, 23
RY Sco	162102	17:50:52.30	-33:42:20	8.0	52	0	0	2.1	1, 22
Z Sct	172902	18:42:57.30	-05:49:15	9.6	41	48	41	3.1	–
S Vul	338867	19:48:23.80	27:17:11	9.1	12	12	37	1.9	–

NOTE—Basic information on the sample of Cepheids discussed. Hipparcos identifiers are given where no HD number was available. Coordinates and mean magnitudes are based on the information from the GCVS^a, average magnitudes are approximate. The number of observations obtained with *Coralie*, *Hamilton*, and *Hermes* are listed together with the total temporal baseline Δt_{obs} of our new observations. Typically, we obtained three observations per pointing with the *Hamilton* spectrograph. The total number of new observations made available here is 1630.

References—References for work previously discussing the binarity or cluster membership of these objects are as follows (see also the binary Cepheids database by Szabados (2003)): 1: Evans & Udalski (1994), 2: Szabados (1996), 3: Casertano et al. (2016), 4: Turner (1977), 5: Anderson et al. (2013), 6: Perryman & ESA (1997), 7: Coulson (1983), 8: Petterson et al. (2004), 9: Madore (1977), 10: Madore & Fernie (1980), 11: Walraven et al. (1964), 12: Lloyd Evans (1968), 13: Stobie (1970), 14: Pel (1978), 15: Szabados (1989), 16: Kurochkin (1966), 17: Szabados (1991), 18: Szabados et al. (2012), 19: Fernie et al. (1966), 20: Vinko (1991), 21: Bersier (2002), 22: Proust et al. (1981), 23: Turner et al. (1993). Sections discussing individual Cepheids in more detail are indicated in the column Refs.

^a<http://www.sai.msu.su/gcvs/gcvs/>

particular importance to this work. $\phi = 0.0$ is expected to be close to a time of maximum light although the values of E presented here are not necessarily comparable to times of maximum light determined from light curves. Similarly, the values of P_{puls} that minimize scatter of the present RV data are close, albeit not necessarily identical, to P_{puls} listed in the literature, depending on the number of harmonics used for the fit as well as how well the pulsations repeat over time. One exception to this procedure is the case of YZ Carinae, where the strong orbital RV signal complicates the determination of P_{puls} based on RV data alone. We therefore used

V-band photometric data from the All Sky Automated Survey (Pojmanski 2002) to derive a new best-fit P_{puls} and adopted this value for the RV modeling.

In general, RV orbital motion is modeled as a Keplerian with semi-amplitude K , eccentricity e , argument of periastron ω , and the true anomaly θ (see e.g. Hilditch 2001):

$$v_{r,\text{orb}} = K [\cos(\omega + \theta) + e \cos \omega]. \quad (3)$$

However, the majority of Cepheids considered here do not exhibit evidence of orbital motion, and indeed one of the primary aims of this work is to set upper limits on undetected companions. We thus assume zero ec-

Table 2. Example RV data obtained for this program

Cepheid	BJD−2.4M [d]	ϕ_{puls}	v_r [km s ^{−1}]	$\sigma(v_r)$ [km s ^{−1}]	Instrument
SY Aur	56402.68783	0.0580	-10.248	0.2	Hamilton
SY Aur	56519.01162	0.5236	6.516	0.2	Hamilton
SY Aur	56519.01798	0.5242	6.500	0.2	Hamilton
SY Aur	56581.00590	0.6341	10.463	0.2	Hamilton
SY Aur	56581.01220	0.6347	10.463	0.2	Hamilton
SY Aur	56581.01850	0.6354	10.496	0.2	Hamilton
SY Aur	56581.91266	0.7235	7.004	0.2	Hamilton
SY Aur	56581.91897	0.7241	6.930	0.2	Hamilton
SY Aur	56581.92527	0.7247	6.837	0.2	Hamilton
SY Aur	56609.97389	0.4894	4.237	0.2	Hamilton
...					
S Vul	57500.899168	0.7406	15.663	0.032	Coralie
S Vul	57504.910489	0.7991	14.473	0.073	Coralie
S Vul	57507.895237	0.8426	10.209	0.035	Coralie
S Vul	57508.895744	0.8572	7.892	0.029	Coralie
S Vul	57511.898062	0.9010	-0.430	0.032	Coralie
S Vul	57526.868106	0.1192	-10.978	0.016	Coralie
S Vul	57528.902885	0.1489	-9.989	0.022	Coralie
S Vul	57529.903860	0.1635	-9.466	0.025	Coralie
S Vul	57534.837524	0.2105	-6.426	0.014	Coralie
S Vul	57536.886856	0.2399	-5.069	0.024	Coralie

NOTE—The full dataset comprising 1630 observations of the 19 Cepheids obtained with the three spectrographs is published online via the Journal and the CDS. Pulsation phase is defined such that $\phi_{\text{puls}} = 0$ at minimal RV and is computed using ephemerides listed in Tab. 3. Dates and RVs are relative to the Solar system barycenter.

centricity unless required (and explicitly stated). This simplifies Eq. 3 to an ordinary sinusoid with amplitude and phase, which we here model as:

$$v_{r,\text{orb},e=0} = a_{\text{orb}} \sin 2\pi\phi_{\text{orb}} + b_{\text{orb}} \cos 2\pi\phi_{\text{orb}}, \quad (4)$$

with orbital semi-amplitude $K = \sqrt{a_{\text{orb}}^2 + b_{\text{orb}}^2}$. Orbital period and semi-amplitude then yield the projected semimajor axis $a \sin i$ of the Cepheid’s orbit around the common center of gravity:

$$a \sin i [\text{AU}] = 9.192 \times 10^{-5} \cdot K [\text{km s}^{-1}] \cdot P_{\text{orb}} [\text{d}]. \quad (5)$$

Highly eccentric or very long orbital period ($P_{\text{orb}} \gg 5 \text{ yr}$) systems may remain undetected by our RV measurements, depending on the geometry and which part of the orbit would be sampled by the observations. To this end, we also inspect the long-term stability of v_γ using a combination of our new data with published RVs from the literature, see §4.3. However, companions on

such very long-period orbits ($P_{\text{orb}} > 10 \text{ yr}$) are not likely to affect the *HST/WFC3* parallax measurements.

In the following subsections, we discuss the pulsational RV modeling of the program Cepheids. The search for spectroscopic binarity and estimation of parallax error due to companions is presented in §4 below.

3.2. RV variability of program Cepheids

Figure 1 presents the data for 18 of the program stars (YZ Car is described separately in Sec. 4.2) together with the fitted pulsation model. Figure 2 shows the corresponding residuals as a function of observation date. The figures illustrate that most Cepheids have very well-sampled RV curves, although a few cases could benefit from better phase-sampling. This includes in particular S Vul, which is observationally challenging due to its extremely long and unstable pulsation period (Makarenko 1978; Mahmoud & Szabados 1980). We here find a best-fit period of $P_{\text{puls}} = 69.7 \text{ d}$, which is approximately 1.4%

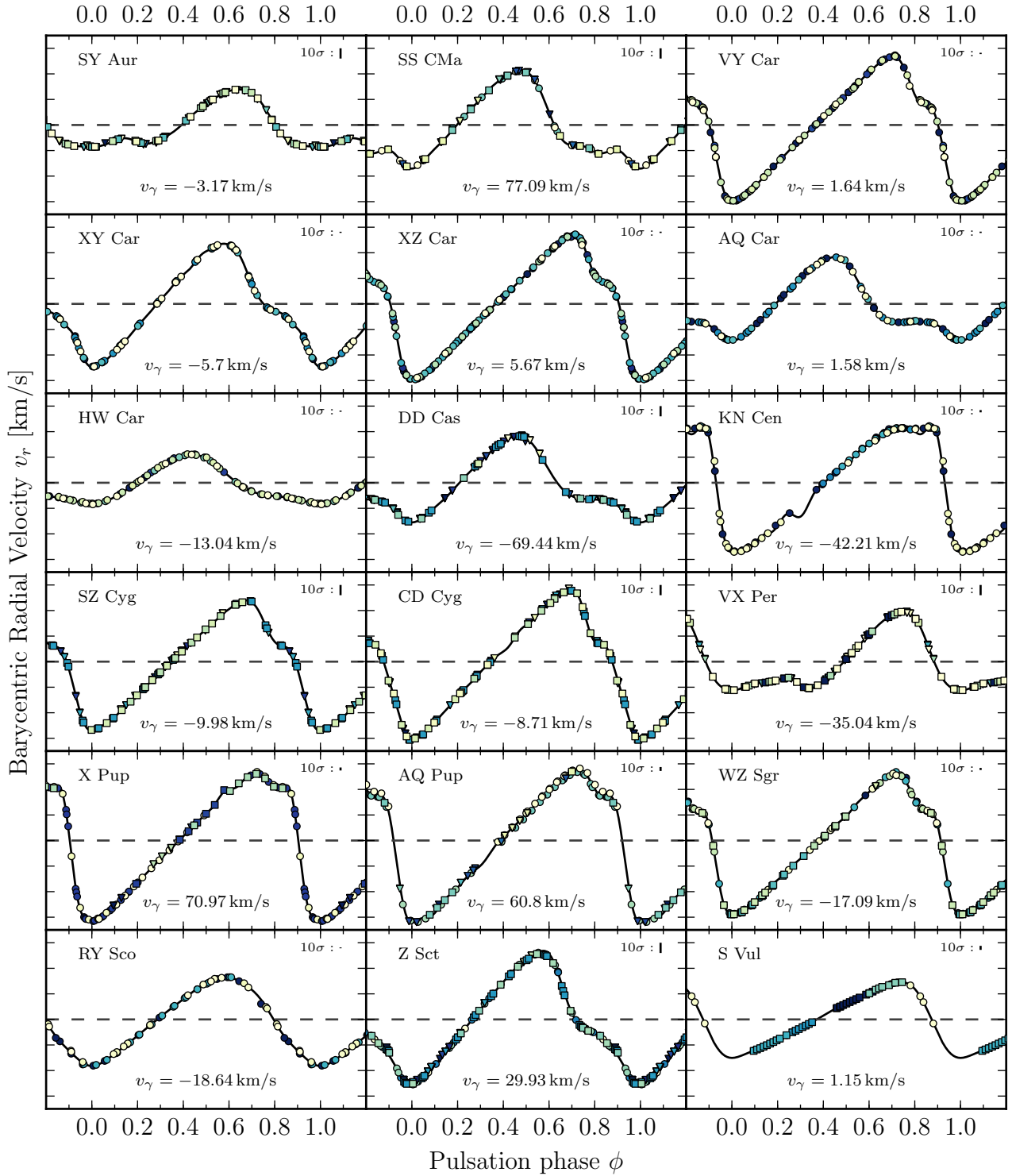


Figure 1. Phase-folded new RV measurements with fitted Fourier series. Color traces observation date increasing from blue to yellow, cf. Fig. 2. The dashed horizontal line indicates v_γ and each subplot's y-range is $v_\gamma \pm 35 \text{ km s}^{-1}$. The ten-fold median uncertainty is indicated in each upper right corner. Circles identify data from *Coralie*, squares from *Hermes*, and triangles from the *Hamilton* spectrograph.

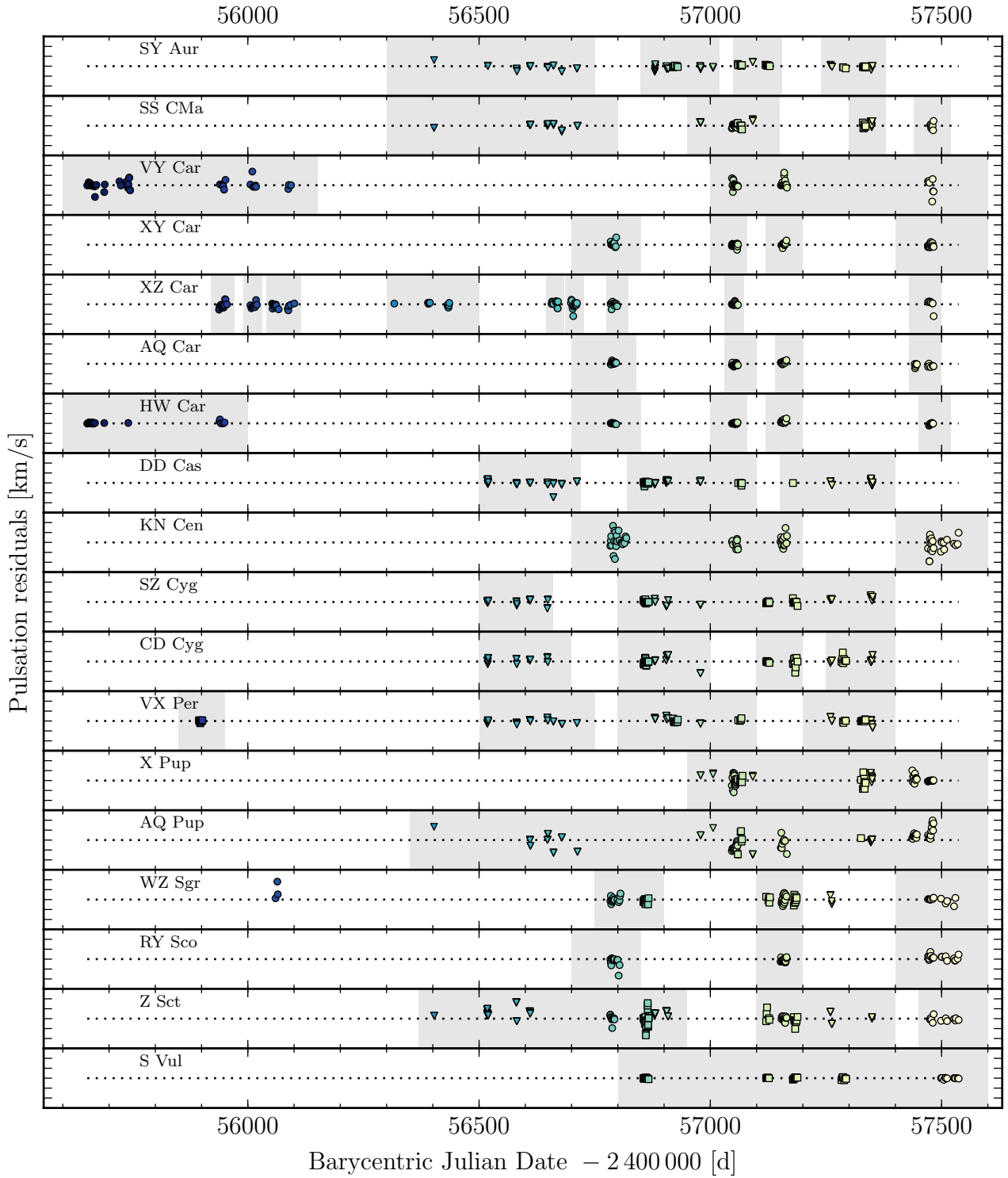


Figure 2. RV residuals after pulsation modeling against (solar system) barycentric Julian date. The ordinate of each subplot is centered on 0 km s^{-1} with a range of $\pm 3 \text{ km s}^{-1}$. Date ranges (tranches) suitable for template fitting are indicated by shaded backgrounds, cf. §4.3.

longer than previously reported values, compared to the range of periods in the literature (67.3–68.7 d). Nevertheless, our observations do not sample the complete pulsation curve (in particular the minimum RV), introducing a substantial systematic period uncertainty of ~ 1 d.

The spectroscopic binarity of Cepheids is usually determined by investigating the long-term stability of the pulsation-averaged velocity v_γ . Specifically, all known Cepheid binaries have $P_{\text{orb}} > 1$ yr and $K > 1$ km s $^{-1}$ (cf. Szabados 2003), possible smaller amplitude companions being masked by RV zero-point offsets among different instruments on the order of a few hundred m s $^{-1}$ (cf. Evans et al. 2015) or noise intrinsic to Cepheid RV variability. The consistently flat residuals shown in Fig. 2 thus provide no indication for spectroscopic binarity, leaving only the possibility of very low-amplitude ($K \lesssim 1$ km s $^{-1}$) or very long-timescale ($P_{\text{orb}} \gg 5$ yr) orbital motion. These possibilities are investigated in detail in Sec. 4.

Table 3 lists the results of the pulsational modeling for all program Cepheids. Specifically, it includes best-fit pulsation periods and epochs, number of harmonics used for the Fourier series N_{FS} , systemic velocity v_γ (which will be of use for *Gaia*, see de Bruijne & Eilers 2012), peak-to-peak amplitude A_{p2p} , amplitude of the first harmonic A_1 , Fourier ratios R_{21} , R_{31} , ϕ_{21} , and ϕ_{31} (Simon & Lee 1981), fit rms and uncertainty on v_γ . Amplitude and phase of the i -th harmonic are defined as $A_i = \sqrt{a_i^2 + b_i^2}$ and $\tan \phi_i = b_i/a_i$, and are computed using the coefficients obtained from Eq. 2. Amplitude ratios among harmonics are defined as $R_{i1} = A_i/A_1$, and phase ratios as $\phi_{i1} = \phi_i - i \cdot \phi_1$. Figure 3 illustrates these results and their dependence on logarithmic P_{puls} , ignoring S Vul for which the available RV data were insufficient to reliably determine these parameters.

We find a dependence of Fourier amplitude and phase ratios on P_{puls} in broad agreement with previous observational (Kovacs et al. 1990) and simulation-based results (Aikawa & Antonello 2000). In particular, we recover the general morphology of increasing RV amplitudes that flatten off around 17 days, as well as the associated steep decline in ϕ_{21} . The period distribution of our program Cepheids nicely complements the sample presented by Kovacs et al. (1990), doubling the number of Cepheids in the P_{puls} range upward of 10 days. These parameters will be useful for hydrodynamical modeling of Cepheid variability, although such applications are outside the scope of this work. Here, we use these parameters to show that most Cepheids exhibit the RV variability behavior expected for their P_{puls} .

We note that the RV amplitudes of RY Sco and YZ Car are outliers from the overall trend indicated by the other stars in the sample. Additionally, visual inspection

of the data reveals that the (pulsational part of the) RV curve is more sinusoidal than that of other Cepheids, cf. Fig. 1 and § 4.2 for YZ Car. This simple RV curve shape is quantified as low amplitude ratios between the first three harmonics, cf. parameters R_{21} and R_{31} in Fig. 3. However, it is known from photometric studies that light curve amplitudes can vary considerably at fixed P_{puls} according to the pulsation-average temperature of the Cepheid, i.e., its position in the instability strip (e.g. Antonello & Morelli 1996; Sandage et al. 2009; Kanbur et al. 2010). Inspection of the *ASAS* lightcurves (Pojmanski 2002) of RY Sco and YZ Car shows that both exhibit very similar, saw-tooth-shaped V -band variability with only a very minor bump-like feature near minimum light and similar peak-to-peak amplitude of ~ 0.8 mag. Since other Cepheids in this P_{puls} range exhibit stronger bump features in their light curves and larger RV amplitudes, this suggests a connection between the low RV amplitudes of RY Sco and YZ Car and the weak bumps. We consider a detailed investigation of the connection between RV and light curve shapes to be out of the scope of this work. In the near future, our parallax measurements will help to clarify whether these differences in light and RV curve shapes among Cepheids are related to differences in luminosity.

3.3. Caveats of Cepheid RV curve modeling

Pulsation period changes due to secular evolution—i.e., linear variations on the order of 10–100 s yr $^{-1}$ for solar metallicity Cepheids in the period range 10–50 d (e.g. Anderson et al. 2016a)—are generally not an issue over the less than 5-year temporal baseline of our observations. However, Cepheids are also known to exhibit non-linear pulsation period changes over shorter timescales, and this effect is particularly noticeable for $P_{\text{puls}} \gtrsim 20$ d. (e.g. Szabados 1989, 1991; Berdnikov et al. 2000, 2009; Poleski 2008; Anderson 2014). A well-known example is RS Pup ($P_{\text{puls}} \sim 42$ d), whose non-linear P_{puls} variations can result in phase offsets of up to 20% over the course of 20 years (Berdnikov et al. 2009). For short-period overtone Cepheids, period fluctuations on similar timescales have been found using high-cadence photometry from *Kepler* and *MOST* (Derekas et al. 2012; Evans et al. 2015).

The peak-to-peak RV amplitudes presented here are on the order of 20–60 km s $^{-1}$, cf. Tab. 3. Using instruments featuring extreme long-term instrumental stability and high RV precision on the order of a few m s $^{-1}$, it is now possible to detect pulsation irregularities on the order of 0.01% with confidence. This has led to the discovery of RV curve modulation (Anderson 2014), which is particularly erratic in long-period ($P_{\text{puls}} > 10$ d) Cepheids, where cycle-to-cycle variations are found. For example, RS Pup’s RV amplitude varies by approxi-

Table 3. Results from RV curve modeling for all program Cepheids

Cepheid	P_{puls} [d]	E JD-2.4M	N_{FS}	v_{γ} [km s $^{-1}$]	A_{p2p} [km s $^{-1}$]	A_1 [km s $^{-1}$]	R_{21}	ϕ_{21}	R_{31}	ϕ_{31}	rms [km s $^{-1}$]	$\sigma_{v_{\gamma}}$ [km s $^{-1}$]
SY Aur	10.145458	56990.536188	9	-3.172	22.403	10.524	0.39	4.33	0.09	6.99	0.216	0.051
SS CMa	12.352828	57062.269144	7	77.085	38.345	16.801	0.24	4.80	0.17	1.62	0.274	0.110
VY Car	18.882696	56502.102998	9	1.637	57.358	23.973	0.29	3.01	0.07	5.27	0.438	0.281
XY Car	12.436275	57145.616572	11	-5.698	48.171	20.987	0.03	3.61	0.13	2.78	0.176	0.161
XZ Car	16.652208	56554.510768	13	5.671	56.299	23.788	0.29	3.01	0.07	5.22	0.274	0.150
YZ Car*	18.1676	51928.9358	8	0.844	29.692	14.078	0.08	3.14	0.04	2.19	0.037	0.063
AQ Car	9.769452	57105.87848	7	1.577	32.932	13.976	0.30	5.08	0.17	1.75	0.167	0.121
HW Car	9.199135	56727.566552	7	-13.035	19.284	9.018	0.22	5.05	0.08	1.74	0.128	0.075
DD Cas	9.812156	56871.673758	7	-69.453	33.913	14.486	0.24	5.24	0.17	2.01	0.163	0.039
KN Cen	34.018969	57135.280429	9	-42.217	50.014	22.343	0.33	3.00	0.21	5.93	0.821	0.514
SZ Cyg	15.11133	56921.702556	9	-9.976	51.060	21.949	0.24	2.94	0.06	4.73	0.255	0.051
CD Cyg	17.076041	56946.237797	11	-8.709	58.892	24.724	0.27	3.01	0.05	5.00	0.352	0.083
VX Per	10.882827	56819.055602	7	-35.037	30.790	13.471	0.47	4.45	0.16	7.41	0.224	0.051
X Pup	25.959165	57262.157494	11	70.970	57.069	25.403	0.36	3.00	0.17	5.77	0.430	0.162
AQ Pup	30.182036	57123.479592	9	60.798	59.522	26.096	0.32	2.98	0.14	5.67	0.777	0.375
WZ Sgr	21.850992	57052.286612	11	-17.088	54.919	23.601	0.32	3.05	0.10	5.55	0.370	0.185
RY Sco	20.322084	57172.826932	7	-18.653	34.768	16.375	0.16	2.93	0.01	4.79	0.330	0.294
Z Sct	12.901867	56956.219712	7	29.924	52.156	22.614	0.06	4.09	0.14	2.46	0.590	0.120
S Vul	69.653841	57241.56046	5	1.137	29.766	12.962	0.35	3.12	0.15	6.24	0.070	0.033

NOTE—Pulsation periods and epochs of minimal RV determined for the number of harmonics indicated (N_{FS}). Mean velocity v_{γ} , peak-to-peak amplitude A_{p2p} , first harmonic amplitude A_1 , Fourier amplitude and phase ratios R_{21} , ϕ_{21} , R_{31} , ϕ_{31} , fit rms, and standard mean error on v_{γ} . *: YZ Carinae is a spectroscopic binary, cf. Tab. 5 and Sec. 4.2.

mately 1 km s $^{-1}$ from one pulsation cycle to the next, and up to 3 km s $^{-1}$ over the course of one year. Both effects are also present, albeit weaker, in the 35 d Cepheid ℓ Car.

Very dense time-sampling is required to model non-linear period and amplitude fluctuations on a cycle-to-cycle basis (Anderson et al. 2016b). Cepheids with $P_{\text{puls}} \gtrsim 20$ d are most affected by these difficulties, since non-linear period fluctuations are strongest for these stars and since achieving good phase-sampling is particularly challenging due to practical constraints such as telescope access, weather, and the Moon.

Modeling Cepheid RV variability using the adopted stable model (Eq. 2) thus fails to account for all (astrophysical) signals present in the data, leading to excess residuals and generally very high values of χ^2 . Since these high χ^2 values are the result of model inadequacy, it would be incorrect to scale RV uncertainties, which have furthermore been shown to represent an adequate estimation of RV precision in the sense of the ability to reproduce a central value from multiple measurements (Anderson 2013).

The presence of additional signals dominates the reduction in χ^2 when a further model component is introduced in the fit, such as orbital motion (Eq. 3 or 4). We therefore caution that a detection of spectroscopic binarity should not be claimed based purely on a reduction in χ^2 . Rather, additional (visual) inspection of the data is required and must be weighed against other indicators.

4. INVESTIGATING SPECTROSCOPIC BINARITY

4.1. Constraining parallax error due to orbital motion

Binarity of variable stars can affect parallax measurements primarily in two ways: 1) via *real* positional modulation due to orbital motion that is not accounted for by the astrometric modeling and 2) via *apparent* positional modulation in phase with the variability (e.g. of the Cepheid). Here we are interested primarily in the former effect and how to constrain the related error using RVs. Objects affected by photocenter variations due to variability were denoted as Variability Induced Movers (Wielen 1996, VIMs) in *Hipparcos* and will be considered in future work, since RVs cannot constrain

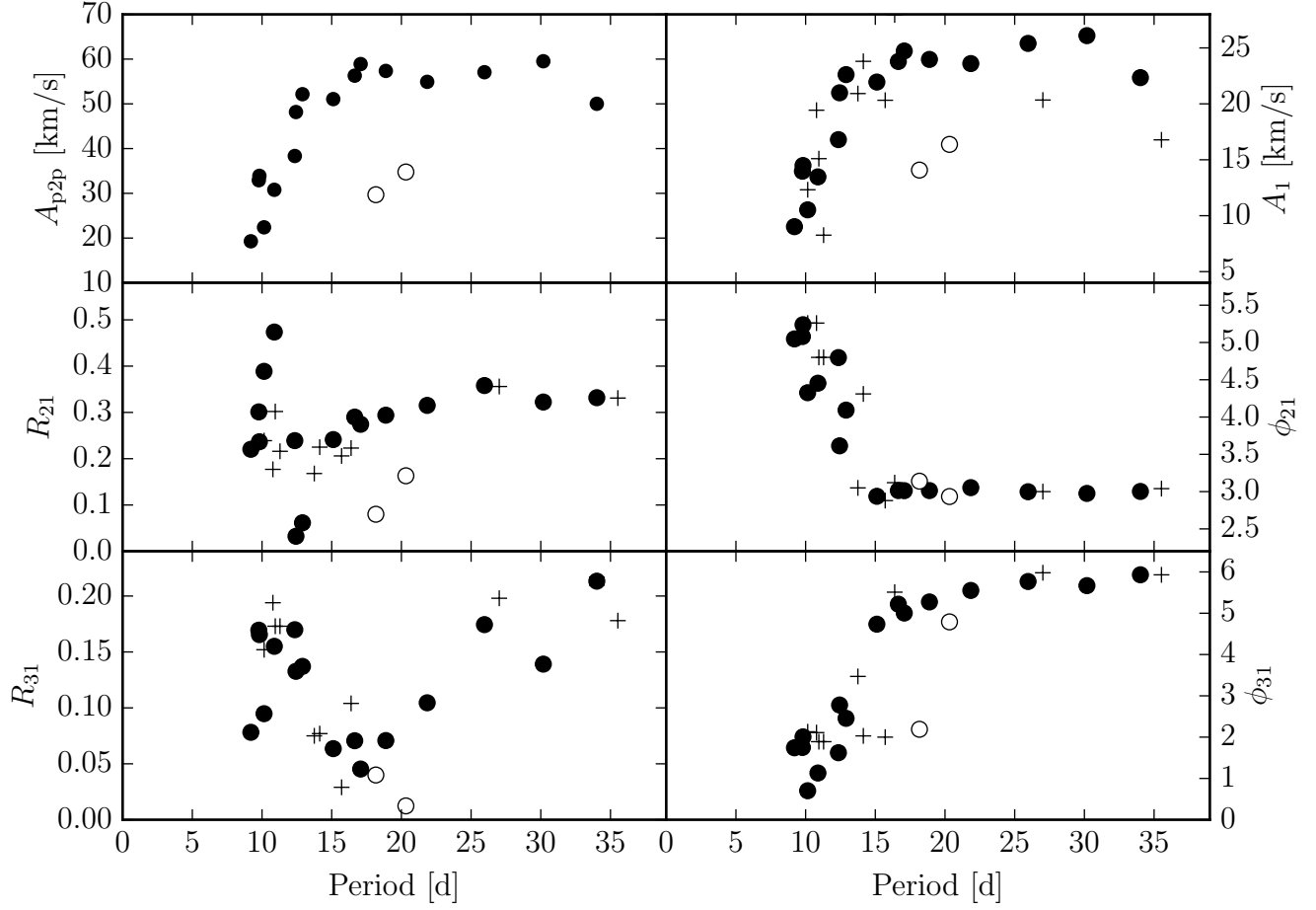


Figure 3. Fourier parameters of the program Cepheids against P_{puls} . SVul ($P_{\text{puls}} \sim 69$ d) is excluded for clarity. YZ Car and RY Sco are marked as open circles. Pluses denote additional Cepheid parameters published by Kovacs et al. (1990).

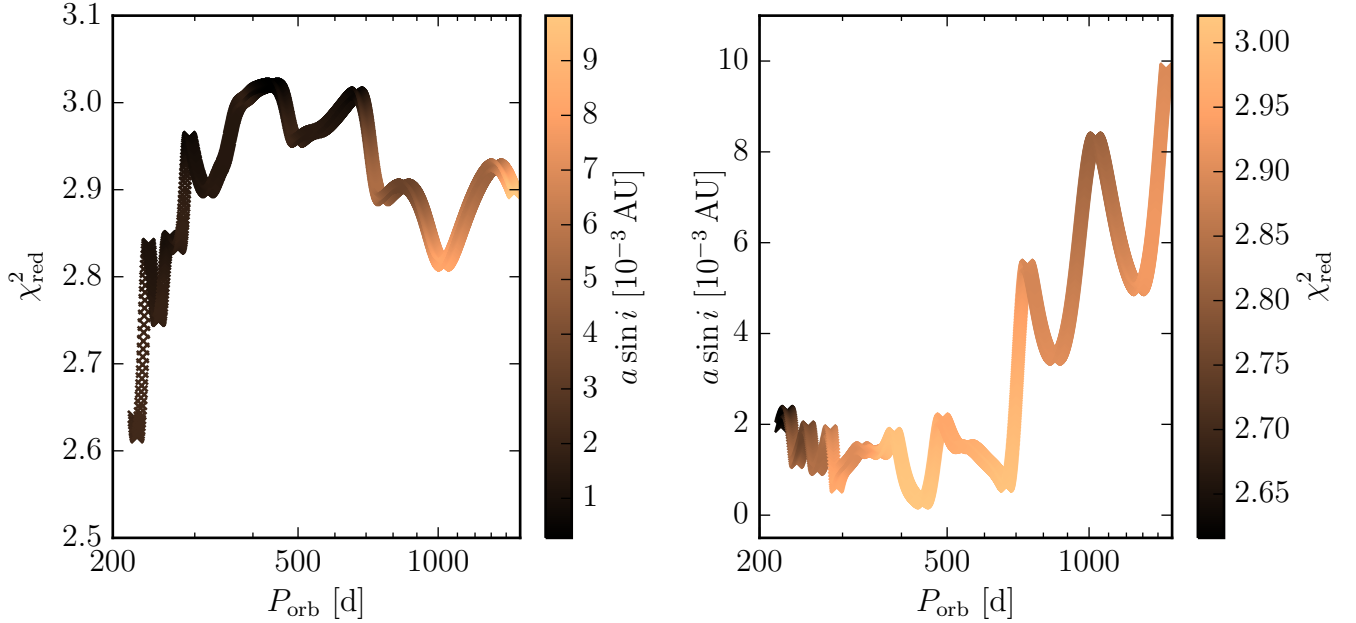


Figure 4. χ^2 map and best-fit projected semimajor axes ($a \sin i$ in [AU]) as a function of (fixed) orbital period for VX Persei.

this effect. It is worth noting that parallax error due to orbital motion can be strong even for low-mass companions that would not lead to VIM-type error, see the example of δ Cep (Anderson et al. 2015) whose companion is at least 5–6 H -band magnitudes fainter than the primary (Gallenne et al. 2016).

Parallax error due to orbital motion (henceforth: parallax error) is expected to be strongest for P_{orb} near one year due to the aliasing between orbital and parallactic motion of the *HST* spatial scan observations. In this section we estimate the possible hidden impact of binarity on the *HST* parallax measurements by determining upper limits on the potential astrometric impact of undetected binaries among the program Cepheids. Photometric effects are briefly discussed in §5.2. We first determine orbital configurations of spectroscopic binaries not ruled out by the high-precision RV data for a range of input orbital periods covering the range of possible binary orbits (here: $P_{\text{orb}} > 222$ d) up to the temporal baseline of the measurements³. We then constrain the parallax error \hat{w} that could result from modeling the *HST* astrometry of the Cepheid as a single star if in reality it were a binary.

The temporal baseline of the RV data presented here is ideal for this purpose. The data have been recorded contemporaneously with (within approximately one year of) the *HST* spatial scan measurements and cover the range of orbital periods where the greatest impact of orbital motion on the parallax measurement is to be expected (longer P_{orb} would primarily affect proper motion). However, while RV data are highly sensitive, they can only measure the line-of-sight component of orbital motion. This limitation is explicitly described in the following.

We model the RV data as a sum of mean velocity, pulsation, and circular orbital motion (Eq. 1 with Eq. 4) for a set of input (fixed) orbital periods P_{orb} using the pulsation ephemerides listed in Tab. 3. For each P_{orb} , we obtain a best-fit solution for v_γ and the Fourier coefficients, as well as a semi-amplitude K and orbital phase ϕ_{orb} . The projected semimajor axis of each best-fit solution is calculated using Eq. 5. We use $a \sin i$ in AU, since the angular size of the orbit scales with the parallax of the Cepheid.

Figure 4 shows the results obtained using this procedure for the example of VX Persei. The left hand panel shows the χ^2 map, which would tend to favor $P_{\text{orb}} < 1$ year with very small $a \sin i$, specified here in [AU], i.e., equivalent to the fraction of the star’s parallax.

To estimate parallax error from these upper limits on spectroscopic binarity, we first compute positional offsets $\delta x(t)$ due to orbital motion at times t of *HST* spatial scan observations using the best-fit values of $a \sin i$ and ϕ_{orb} determined for each P_{orb} . Although RV measurements are blind to inclination, positional offsets due to orbital motion intrinsically depend both on inclination i and the orientation of the line of nodes with respect to the astrometric resolution direction, θ . We therefore compute positional offsets for a two-dimensional grid of inclination and orientation angles for each orbital period P_{orb} used in the RV modeling. Each positional offset is computed as:

$$\delta x(t) = a \cos \phi \cos \theta + a \sin \phi \sin \theta \cos i, \quad (6)$$

where $a = a \sin i / \sin i$ is the semimajor axis of the Cepheid around the center of gravity of the hypothetical binary, and $\phi = 2\pi \frac{t-E}{P_{\text{orb}}} + \phi_{\text{orb},0}$ with E the epoch of the RV modeling (cf. Tab. 3) and $\tan \phi_{\text{orb},0} = B_{\text{orb}}/A_{\text{orb}}$, cf. Eq. 4.

Finally, we estimate the projected parallax error $\hat{w} \sin i$ using the set of positional offsets computed for each orbital period using a least-squares procedure that takes into account the exact times t and parallax factors π_f of each *HST* observation. Hence, we compute $\hat{w}(P_{\text{orb}}, i, \theta)$ using the $\delta x(t)$ for all *HST* observations. As i and θ are unconstrained by the RV data and since we are interested in conservative upper limits, we adopt the maximal unsigned \hat{w} for each P_{orb} and multiply this value by the sine of the inclination for which it was computed, i.e.,

$$\hat{w} \sin i(P_{\text{orb}}) = \max(|\hat{w}(P_{\text{orb}}, i, \theta)|) \cdot \sin i_{\max(|\hat{w}|)} \quad (7)$$

Note that we here use the absolute value $|\hat{w}(P_{\text{orb}}, i, \theta)|$ to estimate the unsigned projected parallax error, since RV data do not constrain i and θ . Depending on the configuration, $\hat{w} \sin i(P_{\text{orb}})$ could be positive or negative, resulting in an over- or underestimated parallax.

The quantity $\hat{w} \sin i$ represents an upper limit in the sense that it reflects the maximal unsigned parallax error for a given orbital period. However, it preserves the notion that the basis for this upper limit, the modeling of RV data, cannot constrain inclination. We further note that $1/\sin i < 3$ for $i > 19.5$ deg (94% of possible inclinations) and < 10 for $i > 5.7$ deg (99.5%).

Table 4 lists the results thus obtained for all program Cepheids excluding YZ Car, whose orbit is updated in §4.2 below. For each Cepheid, we provide information for 1) the solution offering the weakest constraint on possible parallax error, and 2) for the solution with minimal χ^2 .

As mentioned in §3.2 above, we find no indication for binarity for these 18 Cepheids for a range of orbital periods on the order of the observational baseline (2–5 yr, de-

³ All known orbital periods of Cepheid binaries are larger than one year, cf. Szabados (2003); Evans et al. (2015)

pending on the star). More importantly, the minimum- χ^2 solutions provide an estimated mean upper limit on parallax error of 0.8% for all 18 stars ($< 1\%$ for 13, $< 4\%$ for all 18), despite some imperfections in the sampling of some Cepheids. We caution however that the systematic uncertainty of P_{puls} due to incomplete phase coverage may affect the result for SVul, cf. §3.2, although additional observations are required to determine whether this is the case.

The stars with the weakest constraints on $\max(|\hat{\varpi} \sin i|)$ are RY Sco (7%), AQPup (6.7%), XPup (4.2%), and KN Cen (3.1%), all of which exhibit signs of cycle-to-cycle fluctuations of pulsation period and/or amplitude. The 14 remaining Cepheids have $\max(\hat{\varpi} \sin i) < 2\%$, even for these solution with maximal impact. As expected, most of the best-fit orbital solutions that would lead to the greatest parallax error are near the 1 yr alias between orbital and parallactic motion. Both exceptions for which this is not the case, SY Aur and VX Per, yield the largest parallax error at P_{orb} corresponding to the baseline of the measurements. These results therefore strongly suggest that an astrometric modeling assuming a single star configuration is appropriate for all 18 Cepheids, see §4.2 for the exception of YZ Car.

Qualitatively, the flat pulsation-only residuals shown in Fig. 2 already indicated that no large parallax error due to orbital motion was to be expected for these stars. The above results for $a \sin i$ and parallax error mirror and *quantify* this point. While a main limitation of this RV-based work is its insensitivity to inclination, this quantification of possible undetected configurations serves to increase confidence in the accuracy of the parallax measurements themselves and will be useful for future vetting of candidate high-accuracy calibrators of the Galactic Leavitt law.

4.2. Updating the orbital solution of YZ Carinae

YZ Carinae ($P_{\text{puls}} = 18.1676$) is the only spectroscopic binary Cepheid among the program stars whose P_{orb} is shorter than our observational baseline. Its spectroscopic binary nature was discovered and originally reported by Coulson (1983) together with a preliminary orbital estimate of $P_{\text{orb}} \sim 850$ d and low eccentricity. Petterson et al. (2004) obtained additional, higher-precision RV data and determined a significantly shorter orbital period of 657 d with similar eccentricity.

We here update and improve YZ Car’s orbital solution by fitting a combination of a Fourier series and a Keplerian orbit to the new, highly precise, *Coralie* data presented here together with RVs published by Bersier (2002) and the post-1996 measurements by Petterson et al. (2004, Tab. A4). Figure 5 illustrates the quality of this solution. To verify our result, we also deter-

mined the orbit including older measurements by Pont et al. (1994) and Coulson (1983) in the fit, finding excellent agreement. However, these older data do not improve the quality of the solution due to larger measurement uncertainties and/or the possibility of pulsation period changes and we therefore prefer the solution based exclusively on RVs with uncertainties better than 300 m s^{-1} . The value of P_{puls} adopted for this modeling was determined using *ASAS V*-band photometry, since orbital motion significantly affects the measured RV on timescales of a month. Details of YZ Car’s orbital solution and previous determinations are provided in Tab. 5.

The value of $P_{\text{orb}} \sim 830$ d determined here is nearly in agreement with the rough estimate provided by Coulson (1983, 850 d), and strongly disagrees with the solution presented by Petterson et al. (2004, 657.3 d), which is striking due to the small uncertainties quoted in the latter publication. Based on a visual inspection of the various available data sets, we conclude that the pre-1996 data employed by Petterson et al. (2004, Tab. A3) (pre-1996 MJUO RVs) are not comparable with the other available RV data. This mismatch of data could be explained by the fact that the pre-1996 MJUO RVs were measured by different collaborators who may have employed nonstandard definitions of RV, such as bisector velocities, or measured velocities of H α rather than metallic lines (Wallerstein et al. 1992). The fact that the updated result presented here is consistent with all other data spanning nearly 40 years, including Petterson et al.’s post-1996 data strongly supports this conjecture. In addition, we point out the order of magnitude smaller residual scatter in Fig. 5 compared to the scatter of residuals shown in Petterson et al. (2004, Fig. 5).

Using this updated orbital solution together with the actual dates of the *HST* spatial scan observations, we determine $\hat{\varpi} \sin i = 0.26$ AU. Assuming an average inclination of 60 degrees, this would lead to a parallax error of up to 30% (e.g., $\pm 100 \mu\text{arcsec}$ at 3 kpc distance), which should be clearly noticeable in the astrometric measurements. We therefore hope to obtain 2 additional epochs of spatial scan observations of YZ Carinae in order to improve the parallax measurement by accounting for orbital motion in the astrometric model.

4.3. Long-timescale variations of v_γ

Whereas the above sections focus on relatively short timescale orbital motion ($P_{\text{orb}} \lesssim 5 \text{ yr}$), we also investigate longer-term variations of v_γ , which are usually interpreted as evidence for spectroscopic binarity, by comparing our data with older measurements from the literature.

To this end, we divide the available data—literature RVs and our new RVs—into tranches that provide ade-

Table 4. Upper limits on $\hat{\varpi} \sin i$, the maximum unsigned projected parallax error estimated from upper limits on spectroscopic binarity

Cepheid	Δt [yr]	DOF	greatest impact on parallax				overall minimum χ^2					
			P_{orb} [yr]	K [km s $^{-1}$]	$a \sin i$ [% ϖ]	$\hat{\varpi} \sin i$ [% ϖ]	χ^2	P_{orb} [yr]	K [km s $^{-1}$]	$a \sin i$ [% ϖ]	$\hat{\varpi} \sin i$ [% ϖ]	χ^2
SY Aur	2.6	87	2.6	0.186 \pm 0.001	1.63	0.0	125	2.07	0.179 \pm 0.001	1.24	0.0	107
SS CMa	2.96	62	0.76	0.191 \pm 0.022	0.49	0.2	867	0.77	0.193 \pm 0.021	0.5	0.2	866
VY Car	5.01	61	0.95	0.242 \pm 0.028	0.78	0.9	20618	0.64	0.103 \pm 0.008	0.22	0.1	20207
XY Car	1.91	44	1.07	0.421 \pm 0.025	1.52	1.7	3238	1.09	0.43 \pm 0.029	1.58	1.6	3219
XZ Car	4.23	88	0.99	0.185 \pm 0.005	0.61	0.8	10928	2.48	0.197 \pm 0.001	1.64	0.6	8556
AQ Car	1.91	41	1.0	0.476 \pm 0.012	1.6	1.9	709	1.01	0.472 \pm 0.018	1.59	1.9	708
HW Car	5.01	50	0.96	0.149 \pm 0.003	0.48	0.6	789	0.61	0.108 \pm 0.001	0.22	0.1	544
DD Cas	2.28	82	1.05	0.099 \pm 0.001	0.35	0.4	81	1.11	0.1 \pm 0.001	0.37	0.4	80
KN Cen	2.06	47	0.97	0.858 \pm 0.568	2.81	3.1	19831	0.99	0.763 \pm 0.724	2.54	2.8	19791
SZ Cyg	2.28	85	0.96	0.076 \pm 0.001	0.24	0.3	234	1.75	0.147 \pm 0.001	0.87	0.1	204
CD Cyg	2.28	85	1.06	0.122 \pm 0.002	0.43	0.6	552	1.96	0.142 \pm 0.002	0.93	0.2	529
VX Per	3.99	100	3.99	0.073 \pm 0.002	0.98	0.2	290	0.62	0.105 \pm 0.001	0.22	0.0	262
X Pup	1.38	58	1.13	1.168 \pm 0.098	4.43	4.2	2093	1.14	1.128 \pm 0.093	4.31	3.9	2077
AQ Pup	2.96	76	1.01	1.567 \pm 0.047	5.32	6.7	12079	1.66	1.038 \pm 0.004	5.77	0.4	2299
WZ Sgr	4.02	57	0.93	0.222 \pm 0.075	0.69	0.7	5126	1.9	0.406 \pm 0.023	2.59	0.6	4913
RY Sco	2.06	33	0.99	1.901 \pm 1.161	6.34	7.0	13759	0.67	0.41 \pm 0.007	0.93	0.2	13424
Z Set	3.1	111	0.94	0.444 \pm 0.019	1.4	1.5	3156	0.93	0.45 \pm 0.018	1.41	1.4	3148
S Vul	1.87	34	0.97	0.075 \pm 0.005	0.24	0.3	32	0.61	0.192 \pm 0.001	0.39	0.1	27

NOTE—For each star, we list the temporal baseline of our new observations, the degrees of freedom after the fit, as well as best-fit results for a) the orbital solution leading to the maximum unsigned projected parallax error (typically near 1 year orbital period), and b) the orbital solution with overall minimal χ^2 (see Sec. 3.3 for a related discussion). Uncertainties on K are based on the fit covariance matrix. $a \sin i$ is calculated using K and the corresponding fixed P_{orb} (cf. Eq. 5). $\hat{\varpi} \sin i$ is estimated as described in §4.1 and can have positive or negative sign. $\hat{\varpi} \sin i$ and $a \sin i$ are given in [AU], which is equivalent to percent of the parallax. For all solutions shown here, eccentricity $e = 0$. The orbital elements of YZ Carinae are given separately in Tab. 5.

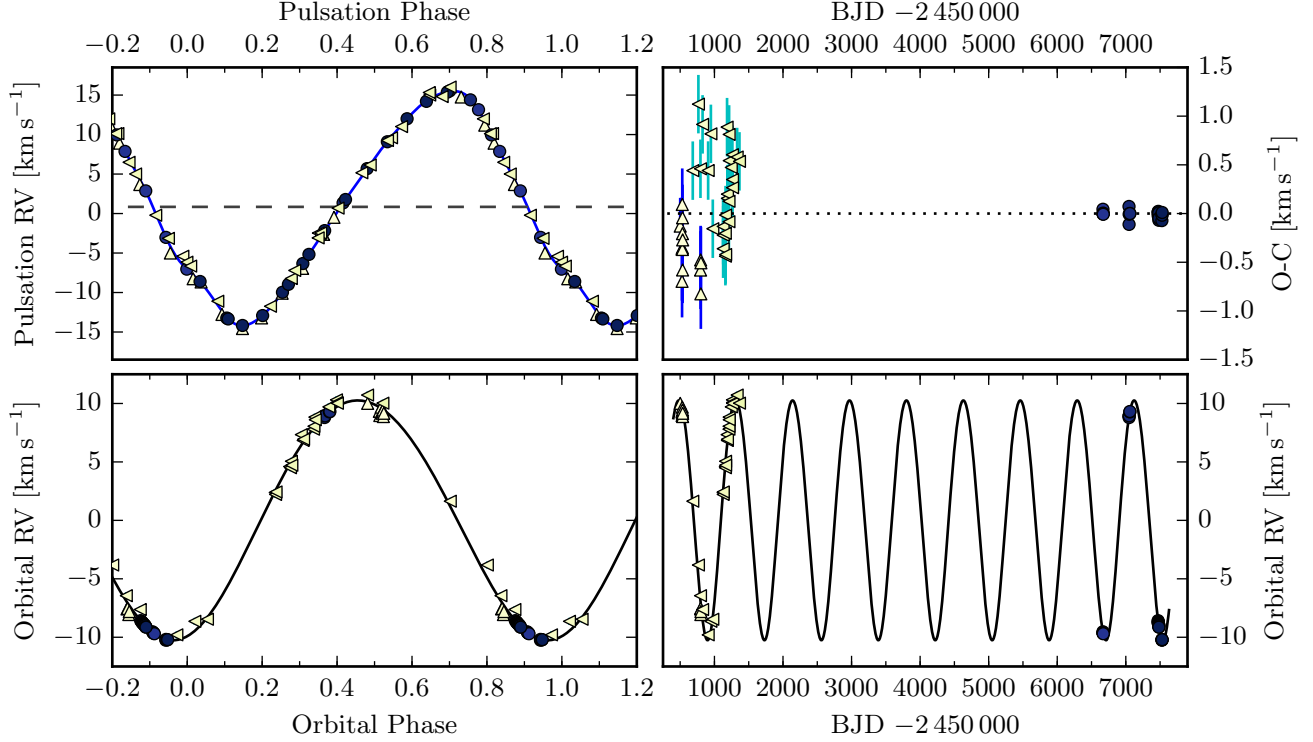


Figure 5. Orbit of YZ Carinae. Color and symbols are the same in all panels. From top left to bottom right: Pulsation-only RV variability incl. systemic velocity 0.844 km s^{-1} indicated by horizontal dashed line; residuals of data minus Fourier series and Keplerian orbit versus observation date; orbital motion phase-folded with orbital period; orbital motion versus observation date. Yellow upward triangles are from [Bersier \(2002\)](#), yellow leftward triangles from [Pettersen et al. \(2004\)](#). Blue circles are *Coralie* measurements.

Table 5. Orbital elements for YZ Carinae

Parameter	C83 ¹	P04 ²	This work
P_{orb} [d]	850 ± 11	657.3 ± 0.3	830.22 ± 0.34
e	0.13 ± 0.07	0.14 ± 0.03	0.041 ± 0.010
K [km s^{-1}]	9.4 ± 0.5	10.0 ± 0.4	10.26 ± 0.82
v_{γ} [km s^{-1}]	1.0 ± 0.4	0.0 ± 0.2	0.844 ± 0.063
$T_0 - 2.4M$	43575 ± 11	42250 ± 9	53422 ± 29
ω [deg]	239 ± 6	116 ± 5	195 ± 12
$a \sin i$ [10^6 km]	—	89	117.1 ± 9.4
f_{mass} [M_{\odot}]	0.071	0.066	0.093 ± 0.041
i_{min} [deg]	—	—	22^{\dagger}
rms [km s^{-1}]	—	—	0.39
$\hat{\omega} \sin i$ [% ϖ]	—	—	26
$\hat{\omega} \sin i / \sin i_{\text{min}}$ [% ϖ]	—	—	76

References—¹: [Coulson \(1983\)](#), ²: [Pettersen et al. \(2004\)](#).

NOTE—Some uncertainties derived here are larger than in the literature due to the combined pulsation plus orbital fit. The minimum inclination (marked by [†]) is determined from the mass function assuming $m_1 = 7 M_{\odot}$. For $m_1 = 9 M_{\odot}$, $\min i = 20 \text{ deg}$.

quate phase sampling, balancing better phase coverage against temporal baseline per tranche. We then determine best-fit P_{puls} , epoch of minimum RV, and v_γ for the data corresponding to each tranche using an RV template fitting approach. To achieve an accurate result it is crucial for the data belonging to a given tranche to sample both the rising and falling branch of the RV curve. The shaded regions in Fig. 2 indicate how data tranches were selected for our new data; literature data were done analogously by inspection of the available data.

The RV templates used to fit each data tranche are created as Fourier series with harmonic coefficients resulting from the pulsational RV curve modeling described in §3.2. Each template fit determines two quantities for a fixed pulsation period $P_{\text{puls}}(t)$: $v_\gamma(t)$, and a phase offset $\delta\phi(t)$ relative to the mean observation date required to determine the time of minimum RV ($E(t)$) corresponding to this tranche and $P_{\text{puls}}(t)$. To account for period changes, we determine the globally best-fitting (minimum χ^2) solution for a grid of input P_{puls} that lie within 0.1 d of the value listed in Tab. 3. We then repeat this procedure to within 0.01 d around the previous best-fit period to achieve a finer result. The final result of each fitted tranche is visually inspected to ensure a satisfactory result.

The main limitations of using time-variable v_γ as an indicator of spectroscopic binarity are 1) RV zero-point offsets among spectrographs and authors (up to several hundred m s^{-1} , see Evans et al. 2015); 2) non-linear period fluctuations preventing adequate phase-folding of a given tranche’s data (can be on the order of 1 km s^{-1} , cf. AQ Pup in § 4.3.2); 3) apparent changes in v_γ induced by cycle-to-cycle changes of RV variability (up to a few hundred m s^{-1} , see Anderson et al. 2016b). Determining the impact of 1) would require precision standard star RV time-series that are generally not available in the literature. Points 2) and 3) are particularly relevant for long-period ($P_{\text{puls}} \gtrsim 20 \text{ d}$) Cepheids as explained in §3.3. To avoid spurious detections, we therefore consider the overall behavior of $v_\gamma(t)$ over all tranches and adopt a threshold of 1 km s^{-1} as the minimum offset before concluding on spectroscopic binarity.

We have thus investigated possible long-term variations of v_γ for 15 of our 18 Cepheids, excluding YZ Car (§4.2), HW Car and S Vul (both: lack of literature data). In the following, we report the discovery of three new candidate spectroscopic binaries (§4.3.1), followed by a critical investigation of Cepheids previously reported to be spectroscopic binaries (§4.3.2). Cepheids reported here or in the literature to be binaries are shown in Fig. 6, whereas Fig. 7 presents Cepheids for which no significant variations in v_γ were found and that have not previously been reported to be binaries.

4.3.1. New candidate spectroscopic binaries

Based on our RV template fitting approach, we report the discovery of three new spectroscopic binary candidates: XZ Car, AQ Car, and CD Cyg; Table 6 lists these results.

Column ‘stdmer’ quotes the standard mean error based on the residual scatter of the fit and should be compared to the fit uncertainty derived from the covariance matrix. It is interesting to note that ‘stdmer’ tends to be smaller than $\sigma(v_\gamma)$ for older, imprecise data, whereas the opposite is the case for new high-precision data. Specifically, the improvement of ‘stdmer’ stagnates compared to the improvement in $\sigma(v_\gamma)$ when using more precise (newer) data to determine v_γ . This is a consequence of the intrinsic astrophysical noise of Cepheid pulsations that manifest as fluctuations in period and RV curve shape (Anderson 2014; Anderson et al. 2016b). Inspection of the v_γ values derived for XZ Car shows that this astrophysical noise can lead to variations larger than a factor of several $\sigma(v_\gamma)$. For XZ Car specifically, the (unweighted) mean v_γ inferred by template fitting of exclusively new measurements is $v_\gamma = 5.603 \pm 0.030 \text{ km s}^{-1}$, which is very close to the value of v_γ determined in a combined Fourier fit (5.671 km s^{-1} , cf. Tab. 3).

Adopting the above-stated threshold of 1 km s^{-1} , we find that XZ Carinae, AQ Carinae, and CD Cygni exhibit significantly time-dependent v_γ on time scales longer than a few years. This marks the first discovery of XZ Car’s binarity, and our new data are decisive in demonstrating the likely binary nature of CD Cyg, which was previously considered not to be a spectroscopic binary (Evans et al. 2015). While AQ Car’s comparatively small v_γ variation ($\sim 1.5 \text{ km s}^{-1}$) among (Bersier 2002) and our RVs renders this evidence tentative, we note that the larger difference to older RVs ($> 2 \text{ km s}^{-1}$ Coulson et al. 1985; Pont et al. 1994) and in particular the high quality of the Bersier (2002) data that provide a well-constrained fit corroborate an interpretation as evidence for spectroscopic binarity.

We note that none of these three Cepheids are expected to have incurred significant parallax error due to orbital motion, Tab. 4 listing $\leq 1.6\%$ for each of their respective $\max(\hat{\omega} \sin i)$ solutions. However, proper motions estimated using long temporal baselines such as the Tycho-Gaia astrometric solution (Michalik et al. 2015) may be affected by long-timescale orbital motion.

4.3.2. Revisiting previously reported spectroscopic binary candidates

In addition to the new binaries presented above, Figure 6 also shows $v_\gamma(t)$ of seven Cepheids that have previously been considered to be spectroscopic binaries.

We have recently discussed the binarity of

Figure 6. Pulsation-average velocities $v_\gamma(t)$ determined by fitting newly-created RV curve templates. XZ Car, AQ Car, CD Cyg are newly-discovered spectroscopic binary Cepheids, see §4.3.1. SS CMa, VY Car, KN Cen, AQ Pup, SZ Cyg, X Pup, and WZ Sgr have been reported as such in the literature and are discussed in §4.3.2. The red dashed line indicates 0, whereas the green dotted line shows an offset of 1 km s^{-1} , usually taken as indicative of a variation in v_γ due to binarity, cf. §4.3.

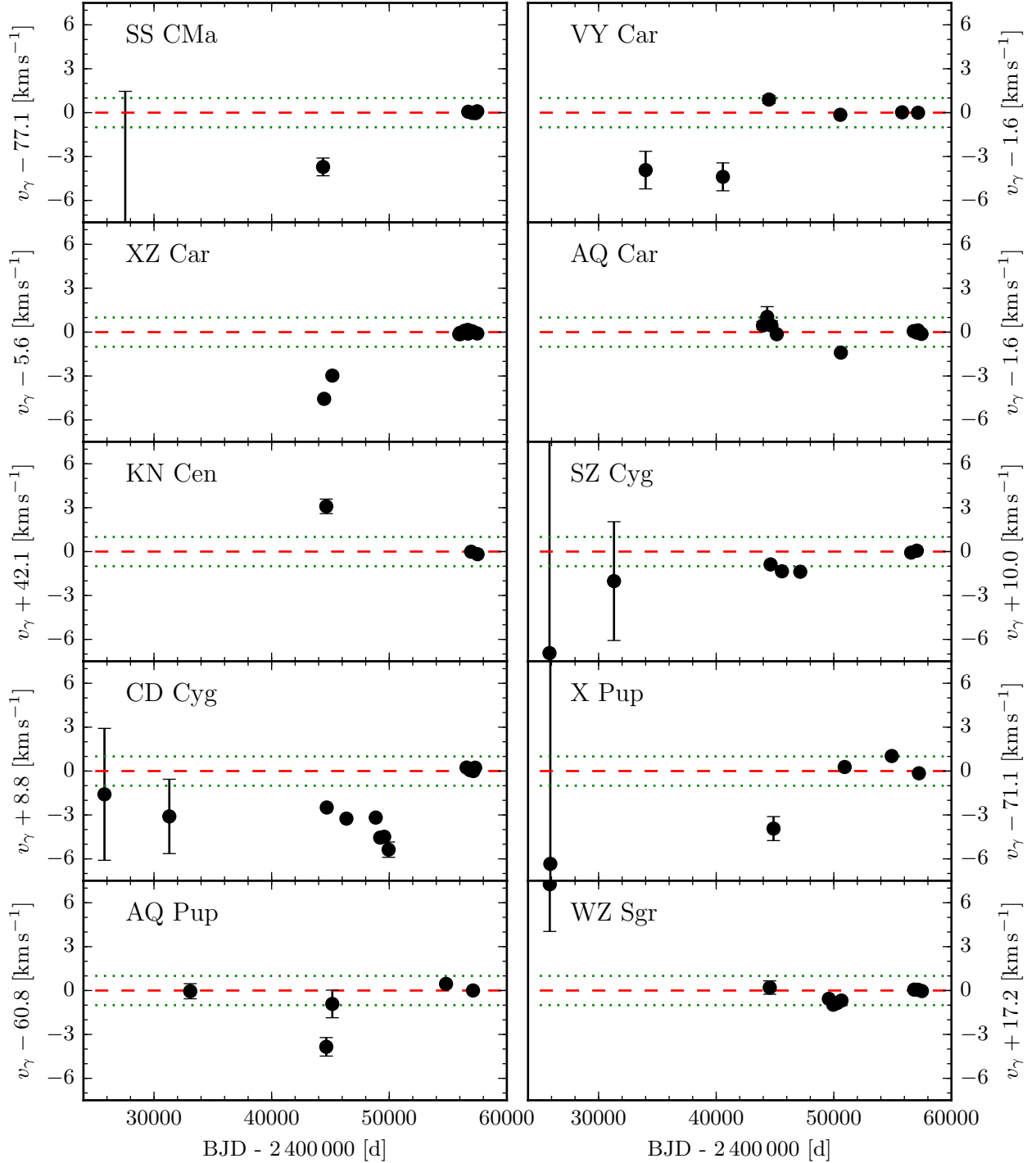


Figure 7. Pulsation-average velocities $v_\gamma(t)$ of Cepheids not exhibiting significant variations in v_γ that have not previously been reported to be spectroscopic binaries. HW Car is not shown here due to a lack of literature data. For VX Per, the epoch near JD 2443000 illustrates the range of possible RV zero-point offsets among instruments via the difference in v_γ inferred using contemporaneous data by [Imbert \(1999\)](#) and [Barnes et al. \(1988\)](#), the latter of which yield a value lower by $\sim 0.8 \text{ km s}^{-1}$.

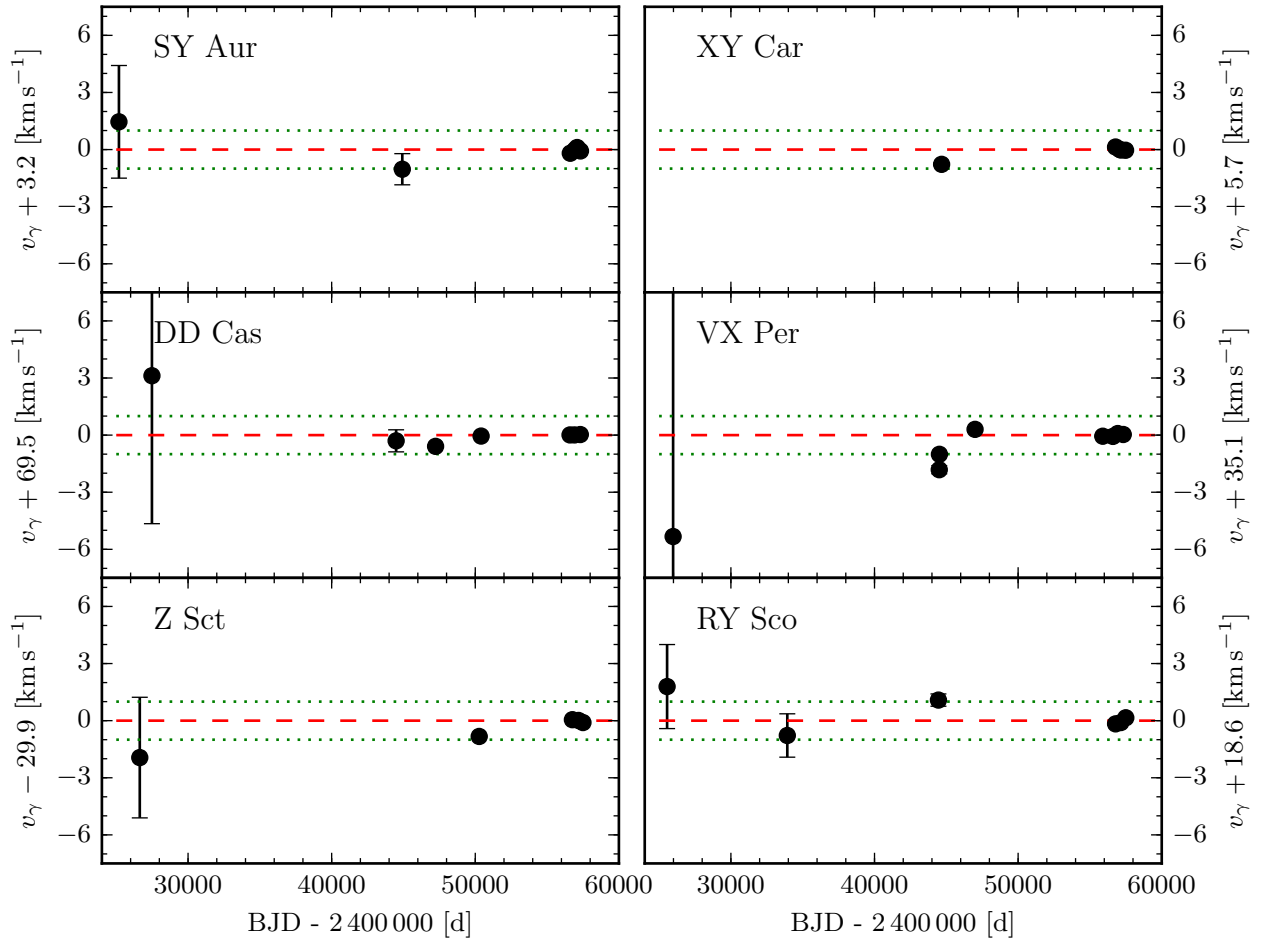


Table 6. Time-variable v_γ of new spectroscopic binaries based on RV template fitting

Cepheid	P_{puls} [d]	Epoch BJD−2.4M	Δt [yr]	N_{RV}	v_γ [km s ^{−1}]	stdmer [km s ^{−1}]	$\sigma(v_\gamma)$ [km s ^{−1}]	References
XZ Car	16.6525	44464.9312	2.21	38	1.07	0.22	0.16	CCG
XZ Car	16.6565	45164.0712	0.98	13	2.66	0.41	0.18	CCG; PBM
XZ Car	16.6573	55955.0183	0.05	15	5.49	0.36	0.003	h
XZ Car	16.6507	56021.6499	0.04	9	5.58	0.23	0.003	h
XZ Car	16.6495	56054.9312	0.04	11	5.55	0.26	0.003	h
XZ Car	16.6549	56088.2126	0.04	5	5.51	0.27	0.001	h
XZ Car	16.6523	56404.6109	0.33	12	5.72	0.18	0.001	h
XZ Car	16.6473	56671.0475	0.04	12	5.78	0.36	0.002	h
XZ Car	16.6473	56704.3392	0.04	14	5.53	0.39	0.004	h
XZ Car	16.6569	56787.6148	0.04	14	5.63	0.26	0.001	h
XZ Car	16.6549	57054.0691	0.04	19	5.69	0.21	< 0.001	h
XZ Car	16.6541	57486.9476	0.03	7	5.54	0.46	0.011	h
AQ Car	9.7745	43975.7970	0.02	8	2.03	0.32	0.27	CCG
AQ Car	9.7717	44337.1307	0.58	18	2.61	0.49	0.70	CCG
AQ Car	9.7689	44698.7272	0.51	25	2.02	0.32	0.32	CCG
AQ Car	9.7679	45148.1286	1.32	19	1.43	0.17	0.018	CCG; PBM
AQ Car	9.7677	50599.3879	0.83	15	0.17	0.21	0.015	B02
AQ Car	9.7679	56793.2563	0.03	13	1.64	0.20	0.001	h
AQ Car	9.7705	57057.0354	0.04	21	1.54	0.14	< 0.001	h
AQ Car	9.7673	57154.7358	0.03	13	1.69	0.15	0.001	h
AQ Car	9.7698	57457.5769	0.11	12	1.45	0.26	0.002	h
CD Cyg	17.075	25787.5216	5.19	12	-10.39	1.07	4.51	J37
CD Cyg	17.081	31301.5552	0.07	22	-11.90	0.63	2.54	S45
CD Cyg	17.0759	44686.6171	2.66	30	-11.29	0.22	0.020	I99; B88
CD Cyg	17.0758	46359.9408	3.54	10	-12.05	0.38	0.044	I99
CD Cyg	17.079	48852.8005	0.27	19	-11.98	0.37	0.051	G92
CD Cyg	17.071	49228.4290	0.15	6	-13.35	0.66	0.093	G92
CD Cyg	17.071	49569.8434	0.22	9	-13.29	0.36	0.055	G92
CD Cyg	17.081	49945.3098	0.12	12	-14.17	0.58	0.52	G92
CD Cyg	17.0792	56570.5614	0.36	30	-8.56	0.09	0.001	h
CD Cyg	17.0748	56877.9332	0.34	39	-8.74	0.13	0.001	h
CD Cyg	17.0742	57151.1361	0.19	17	-8.80	0.19	0.003	h
CD Cyg	17.0752	57304.8482	0.25	25	-8.57	0.13	0.001	h

References—CCG: [Coulson et al. \(1985\)](#), PBM: [Pont et al. \(1994\)](#), B02: [Bersier \(2002\)](#), J37: [Joy \(1937\)](#), I99: [Imbert \(1999\)](#), B88: [Barnes et al. \(1988\)](#), S45: [Struve \(1945\)](#), G92: [Gorynya et al. \(1992\)](#), h: this work.

NOTE— P_{puls} , E, and v_γ are based on RV template fitting. Δt indicates the timespan of the measurement, N_{RV} the number of measurements fitted, ‘stdmer’ the standard mean error based on residual scatter, $\sigma(v_\gamma)$ the uncertainty from the fit covariance matrix.

SS Canis Majoris in light of our *HST* astrometric and recent high-precision RV measurements (Casertano et al. 2016). Using our RV template fitting technique, we here additionally investigate long-term variations of v_γ not discussed in our preceding paper. We find that the oldest data by Joy (1937) are not sufficiently accurate to determine v_γ with precision, although the central values of our fit results do reproduce the difference of $\sim 15 \text{ km s}^{-1}$ compared to RV data by Coulson & Caldwell (1985) as previously reported (Szabados 1996). Using Coulson & Caldwell’s data, we determine a significant offset in v_γ of $\sim 3.8 \text{ km s}^{-1}$ compared to our new data, cf. Tab. 7, which would support a long-timescale spectroscopic binary nature of SS CMa.

KN Centauri is a special case among binary Cepheids in that its hot main sequence companion has been detected and characterized using optical photometry (Madore 1977; Madore & Fernie 1980) as well as UV (Böhm-Vitense & Proffitt 1985; Evans 1994) and optical (Lloyd Evans 1980) spectra. However, the orbital signature on the RV curve had thus far escaped detection. We here report a detection of this signature based on the $\sim 3 \text{ km s}^{-1}$ offset in v_γ , cf. Tab. 7. The potential ability to detect the orbital motion of both components separately renders KN Cen an important target for a future model-independent mass measurement.

VY Carinae is a cluster Cepheid (Turner 1977; Anderson et al. 2013) whose previously reported spectroscopic binarity was based on evidence for low-amplitude variations of v_γ (Szabados (1996, $2K < 5 \text{ km s}^{-1}$). The variation of v_γ for VY Car shown in Fig. 6 is peculiar: the two oldest epochs indicate a rather constant velocity, and so the four newer epochs. At present, it is difficult to judge whether this pattern is caused by orbital motion or rather due to systematics such as data quality or sampling.

SZ Cygni had previously been reported to exhibit time-variable v_γ by Struve (1945) and Szabados (1991). However, we find that the data upon which this evidence was based do not constrain v_γ at the crucial epochs. Notably, the data by Joy (1937) and Struve (1945) are imprecise and do not sample pulsation phase very well. We do, however, find that data by Imbert (1999) indicate a small difference of about 1.3 km s^{-1} relative to v_γ determined using our new measurements.

X Puppis was first reported to exhibit time-variable v_γ by Szabados et al. (2012). Similarly to SZ Cygni, we find that the oldest RV data are insufficiently accurate and sampled to constrain the fit well. However, data published by Barnes et al. (1988) and Caldwell et al. (2001) yield a significantly lower v_γ than newer measurements, which furthermore exhibit a suspicious trend in $v_\gamma(t)$. Additional high-precision observations of X Pup taken

over the next few years will clarify whether this variation is consistent with orbital motion.

AQ Puppis exhibits very significant non-linear changes of P_{puls} (Vinko 1991) in addition to exceptionally fast (300 s yr^{-1}) secular changes of P_{puls} (Berdnikov & Ignatova 2000) that approach values predicted for Cepheids on a first crossing of the instability strip (Turner et al. 2012; Anderson et al. 2016a). Fernie et al. (1966) reported a chance alignment with an OB association (see also Turner et al. 2012), which the *HST* spatial scans will further illuminate. Madore & Fernie (1980) presented evidence of a photometric companion based on both a phase-shift and color-loop methodology. AQ Pup’s spectroscopic binary nature was reported by (Vinko 1991) based on a systematic offset in mean velocity between the data from Joy (1937) and those by Stibbs (1955), Barnes et al. (1988), and Coulson & Caldwell (1985). Ignoring the imprecise and extremely sparse (5 measurements over 4 years) data by Joy (1937), we find that nearly all available RV data is consistent with a constant v_γ . However, RVs measured near epoch JD 44650 appear to be offset by $\sim 3 \text{ km s}^{-1}$ (cf. Tab. 7 and Fig. 6) from measurements taken just one year later by the same authors (Coulson & Caldwell 1985; Barnes et al. 1988). Following visual inspection of the RV data and given that our new RV data do not indicate fast and significant variations in v_γ , we do not consider this apparent offset in v_γ to be a solid indication of spectroscopic binarity. Rather, it appears more likely that non-linear changes of P_{puls} (see e.g. Turner et al. 2012, Fig. 10) lead to problems in phase-folding the data, which is required to determine v_γ .

WZ Sagittarii is a member of the open cluster Turner 2 (Turner et al. 1993; Anderson et al. 2013), whose other members may aid in the determination of its accurate parallax. A spectroscopic binary nature of WZ Sgr has both been argued for (Szabados 1989) and against (Evans et al. 2015). As Fig. 6 shows, nearly all RV data are nicely consistent with a stable v_γ , the oldest data by Joy (1937, 8 measurements) being the exception. We thus conclude that WZ Sgr is unlikely to be a spectroscopic binary.

5. DISCUSSION

The *Gaia* mission is currently measuring highly accurate parallaxes for hundreds of Galactic Cepheids. This order-of-magnitude increase in sample size compared to the current 12 accurately known Cepheid parallaxes (Benedict et al. 2007; Riess et al. 2014; Casertano et al. 2016) will enable future calibrations of the extragalactic distance scale based on subsamples of Cepheids selected according to properties deemed particularly suitable for this task. To this end, a detailed vetting process that considers the wide range of information available for

Table 7. Time-dependent v_γ based on RV template fitting for reported binary Cepheids

Cepheid	P_{puls} [d]	Epoch BJD−2.4M	Δt [yr]	N_{RV}	v_γ [km s ^{−1}]	stdmer [km s ^{−1}]	$\sigma(v_\gamma)$ [km s ^{−1}]	References
SS CMa	12.3568	27554.7032	3.15	5	58.36	2.51	20.2	J37
SS CMa	12.3536	44373.6734	2.04	47	73.39	0.45	0.61	CC85
SS CMa	12.3528	56716.3689	1.58	27	77.16	0.10	0.002	h
SS CMa	12.3522	57062.2692	0.12	26	77.08	0.17	0.001	h
SS CMa	12.3478	57346.3907	0.06	19	77.07	0.21	0.002	h
SS CMa	12.3478	57482.2462	0.02	8	77.19	0.49	0.014	h
VY Car	18.8865	33999.9783	1.04	15	−2.31	0.59	1.28	S55
VY Car	18.8847	40567.9096	1.08	6	−2.77	0.64	0.95	L80
VY Car	18.8853	44483.7134	3.08	60	2.51	0.30	0.27	CC85
VY Car	18.8841	50551.7748	0.82	16	1.47	0.45	0.064	B02
VY Car	18.8831	55803.4453	1.21	41	1.64	0.41	0.002	h
VY Car	18.8825	57162.9905	1.19	42	1.61	0.26	0.001	h
KN Cen	34.0232	44545.6646	3.08	34	−39.05	0.41	0.50	CC85
KN Cen	34.0192	56965.1895	1.05	47	−42.15	0.48	0.008	h
KN Cen	34.0206	57509.4973	0.18	23	−42.32	0.98	0.036	h
SZ Cyg	15.1127	25826.3093	7.45	8	−16.97	2.26	19.3	J37
SZ Cyg	15.1063	31310.5534	0.07	17	−12.05	0.74	4.06	S45
SZ Cyg	15.1079	44622.2780	2.48	28	−10.91	0.26	0.038	I99; B88
SZ Cyg	15.1112	45589.2646	3.02	18	−11.38	0.17	0.012	I99
SZ Cyg	15.1113	47145.6313	3.29	14	−11.41	0.22	0.016	I99
SZ Cyg	15.1157	56574.1255	0.36	30	−10.10	0.11	0.002	h
SZ Cyg	15.1113	57057.7047	1.36	77	−9.97	0.05	< 0.001	h
X Pup	25.9582	25896.3080	3.98	10	64.78	1.54	14.6	J37
X Pup	25.9628	44874.5896	2.33	32	67.19	0.49	0.82	B88; C01
X Pup	25.9608	50924.8055	2.10	33	71.40	0.33	0.034	B02; P05
X Pup	25.9605	54924.3983	1.23	42	72.15	0.37	0.017	S11
X Pup	25.9602	57235.7830	1.38	84	70.97	0.25	0.002	h
AQ Pup	30.1768	33078.6817	0.45	13	60.75	0.37	0.52	S55
AQ Pup	30.1768	44647.4321	0.49	30	56.95	0.43	0.63	CC85; B88
AQ Pup	30.1834	45159.8310	1.21	14	59.88	0.49	0.94	CC85; B88
AQ Pup	30.1806	54829.5366	1.74	38	61.25	0.70	0.068	S11
AQ Pup	30.1820	57093.2976	2.96	98	60.80	0.34	0.006	h
WZ Sgr	21.8521	25849.9613	5.09	9	−9.91	0.92	3.23	J37
WZ Sgr	21.8549	44553.0330	2.83	24	−16.97	0.37	0.46	CC85; B88
WZ Sgr	21.8461	49578.7275	0.17	26	−17.74	0.30	0.12	G92
WZ Sgr	21.8561	49950.1832	0.27	19	−18.14	0.39	0.05	G92
WZ Sgr	21.8463	50277.9982	0.22	38	−18.03	0.25	0.02	B02; G92
WZ Sgr	21.8535	50649.5795	0.49	32	−17.86	0.25	0.02	B02; G92
WZ Sgr	21.8521	56833.7761	0.23	33	−17.11	0.22	0.001	h
WZ Sgr	21.8507	57161.5552	0.18	29	−17.12	0.36	0.006	h
WZ Sgr	21.8516	57489.2777	0.18	13	−17.21	0.30	0.005	h

References—S45: [Struve \(1945\)](#), CC85: [Coulson & Caldwell \(1985\)](#), L80: [Lloyd Evans \(1980\)](#), B88: [Barnes et al. \(1988\)](#), I99: [Imbert \(1999\)](#), S11: [Storm et al. \(2011\)](#), G92: [Gorynya et al. \(1992\)](#), B02: [Bersier \(2002\)](#), J37: [Joy \(1937\)](#), S55: [Stibbs \(1955\)](#), P05: [Pettersen et al. \(2005\)](#), C01: [Caldwell et al. \(2001\)](#)

NOTE—See also Tab. 6. J37 data do not constrain the fit well for SS CMa, SZ Cyg, and X Pup.

Galactic Cepheids is required. We consider the vetting process of Galactic Leavitt law calibrators to be a crucial step towards a measurement of H_0 with 1% accuracy.

The investigation of binarity is an important element of this vetting process. In this work, we focus on the contribution that RV measurements can make in this regard. Specifically, we use RVs to constrain possible parallax error due to orbital motion for our *HST* parallaxes (Riess et al. 2014; Casertano et al. 2016). This is very important, since the typically 5 observed *HST* epochs do not provide sufficient degrees of freedom to determine position, proper motion, parallax⁴ and orbital motion simultaneously. Hence, this work informs the systematic uncertainty budget of the *HST* spatial scan parallaxes and increases confidence in their accuracy.

Our work demonstrates that RVs are very well-suited for investigating this parallax error, since they provide tight constraints on the range of orbital periods that would most impact the parallax measurements (1–3 yr), despite their insensitivity to inclination. This is because the orbital RV signal for a given P_{orb} and e depends on the mass function $((m_2 \sin i)^3 / (m_1 + m_2)^2)$ of the binary. Another method capable of investigating such short-period systems is optical/NIR long-baseline interferometry. However, the ability to detect companion stars interferometrically depends on the luminosity contrast (Gallenne et al. 2015, feasible dynamic range of 1 : 200), which tends to be very high due to the evolutionary differences between a Cepheid and its typically main sequence companion, cf. §5.2, as well as the nature of the mass-luminosity relation.

Our RV-based results presented here indicate that orbital motion-induced parallax error is insignificant for most (18 of the total 19) Cepheids in the sample thanks to tight upper limits on undetected orbital configurations. Since it is highly unlikely for a large fraction of Cepheids to have nearly face-on orbits ($1/\sin i < 3$ for 94% of possible i values), we do not expect more than one of these 18 Cepheids to be subject to (projection-corrected) parallax error due to orbital motion exceeding $\pm 10\%$ and we have at present no indication of any such error.

The exception among our sample stars is YZ Carinae whose orbit is clearly detected and expected to significantly affect parallax ($\hat{w} \sin i \sim \pm 100 \mu\text{arcsec}$). Additional spatial scans will be obtained for this star in order to allow our astrometric modeling to account for orbital motion. Correcting the orbital solution (cf. §4.2) was

crucial to provide adequate constraints to this effect.

The method described here can also be applied to RVs measured using *Gaia*'s *RVS* instrument provided that time-series RVs are sufficiently precise to provide stringent constraints on undetected orbital configurations. However, *Gaia* has the advantage of gathering an average of ~ 70 astrometric measurements per star and is therefore able to directly include orbital motion in the astrometric modeling. Further ground-based observations are being secured to assist an investigation of binarity in support of *Gaia*.

The long-timescale ($P_{\text{orb}} \gg 5 \text{ yr}$) spectroscopic binaries reported in §4.3 are not expected to affect our *HST* parallax measurements. However, proper motion measurements may be affected by such long-period orbital motion.

Of course, the impact of binarity on the distance scale is not limited to parallax measurements and stands to benefit from an investigation of data other than purely RV observations. Conversely, other known properties of Cepheids (besides binarity) deserve detailed investigation in terms of their impact on the calibration of the distance scale. In the following, we provide an overview of considerations to be made by such a vetting process directly related to the present work.

5.1. Binary frequency in this sample

The Cepheid binary fraction has been a topic of intense research for several decades (e.g. Lloyd Evans 1968; Madore 1977; Böhm-Vitense & Proffitt 1985; Szabados 1991; Evans & Udalski 1994; Evans et al. 2015, 2016b,a). Yet, inspection of the available literature data of previously reported candidate binaries (cf. §4.3) and the discovery of previously unknown binary systems among our relatively bright Cepheids suggests that far from everything is known for even relatively well-studied cases.

As mentioned in §2.1, the present sample of Cepheids is not random with respect to binarity and may therefore not be representative of the binary fraction of all Cepheids. Nevertheless, we summarize our investigation of binarity for the program Cepheids. Convincing evidence for spectroscopic binarity for 5 of 19 Cepheids (SS CMa, YZ Car, XZ Car, KN Cen, and CD Cyg). Four additional Cepheids (VY Car, AQ Car, SZ Cyg, X Pup) exhibit tentative evidence of variations in v_γ consistent with binarity, although imprecise literature data and sometimes heavily fluctuating pulsational variability renders these results inconclusive. The literature further indicates DD Cas to have an unresolved photometric companions (this applies also to KN Cen), bringing the total number of binaries in this sample to between 6/19 (32%) and 10/19 (53%), depending on the inclusion of questionable candidates. This is broadly consistent

⁴ note that five degrees of freedom are sufficient to constrain these parameters, since spatial scan measurements are one-dimensional by construction, cf. Riess et al. (2014)

with other recent estimates, e.g. by Neilson et al. (2015, 35%) and Evans et al. (2015, $29 \pm 8\%$ for $P_{\text{orb}} < 20$ yr). These numbers do not include previously reported cases of visual binaries with extreme separations (greater than a couple arcseconds) or Cepheids belonging to open clusters.

Furthermore, we stress that not all binary Cepheids are fundamentally unsuitable as high-accuracy Leavitt law calibrators, provided their photometry is not biased (cf. §5.2) and that parallax can be measured accurately (cf. §4.1). Additional photometric and interferometric observations will be useful to investigate these points.

5.2. Photometric bias due to companions

The literature contains frequent references to binarity as being a significant source of photometric bias for the estimation of absolute magnitudes. For distance scale applications, this leads to two main questions: 1) what is the (pulsation-phase) average contrast between a Cepheid and a typical companion star? 2) how large of an effect on the distance scale could result from systematic differences in binary statistics among selected samples of Galactic and extragalactic Cepheids?

We therefore estimate the photometric contrast between Cepheids and typical, spatially unresolved, hot main sequence companions via isochrones computed using the Geneva stellar evolution group’s (Ekström et al. 2012; Georgy et al. 2013) online tool⁵. We estimate the luminosity of the hot companion assuming a fixed mass ratio of $q = m_2/m_1 = 0.7$ as a conservative typical value based on the extensive work by N. Evans and collaborators (e.g. Evans 1995; Evans et al. 2013). For KN Cen and DD Cas, we use information on detected companions (Madore 1977) to estimate worst case scenarios. Specifically, we assume a brighter B2 companion for KN Cen, despite *IUE* spectra indicating a B6 dwarf (Evans 1994). Masses are referred to here as lower case m to distinguish them from magnitudes M . The mass of the Cepheid is determined via a (pulsation) period-mass relation based on Geneva models (Anderson et al. 2016a) and thus sets the mass scale for both stars. The age of the isochrone is adopted based on period-age relations by Anderson et al. (2016a) using period change information measured or compiled by Turner et al. (2006) to inform the crossing number, where possible. The isochrone is computed for the inferred Cepheid’s age, solar metallicity, and typical ZAMS rotation rate ($\omega = 0.5$). The contrast in different pass-bands and filter combinations is estimated by forcing the Cepheid to be observed during blue loop evo-

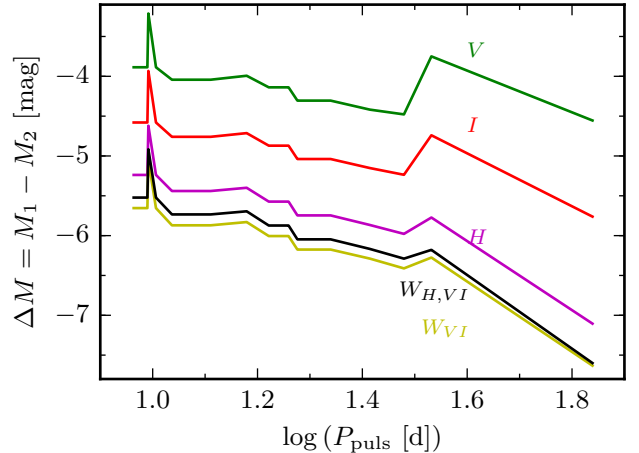


Figure 8. Magnitude difference between Cepheid and main sequence companion (cf. Tab. 8) in different photometric pass-bands based on Geneva isochrones.

lution and looking up the properties of the companion with mass close to m_2 as per the adopted mass ratio. All hypothetical companions thus investigated are hot main sequence stars.

Using this approach, we estimate approximate magnitude differences in bolometric magnitudes, *V*-band, *I*-band, *H*-band, as well as reddening-free Wesenheit indices (Madore 1982) $W_{VI} = I - 1.55(V - I)$ (Soszyński et al. 2008) and $W_{H,VI} = H - 0.4(V - I)$ (Riess et al. 2011), which are known to be particularly useful for measuring Cepheid distances using PLRs thanks to reduced intrinsic PLR dispersion and reduced sensitivity to reddening⁶.

Table 8 lists the results obtained, including the adopted crossing number as well as inferred age and primary (Cepheid) mass m_1 . The remaining columns list the quantities of the companion.

Figure 8 illustrates the comparison. It clearly shows that the contrast between Cepheid and companion increases with increasing wavelength. DD Cas and KN Cen stand out as spikes against the general trend due to higher mass ratios. Wesenheit indices amplify the contrast since Cepheids tend to be much redder than their hot main sequence companions. Fig. 8 further suggests a P_{puls} -dependence of this contrast that can be understood via the larger luminosity difference between stars on main sequence and blue loop evolutionary phases for younger (higher P_{puls}) stars compared to older (lower P_{puls}) stars.

While a more detailed investigation of this effect would require population synthesis and examination of Cepheid colors and binary properties, we here note that

⁵ <http://obswww.unige.ch/Recherche/evoldb/index/Isochrone/>

⁶ Wesenheit magnitudes are “reddening-free” by construction provided the reddening law is known sufficiently well

Table 8. Estimating typical photometric bias due to main sequence companions

Cepheid	Xing	age	log age	m_1	— assumes $m_2/m_1 = 0.7$ —					
					m_2	ΔM_V	ΔM_I	ΔM_H	ΔW_{VI}	$\Delta W_{H,VI}$
SY Aur	3	81	7.91	6.0	4.2	-3.89	-4.58	-5.24	-5.65	-5.52
SS CMa	0	68	7.83	6.3	4.4	-4.04	-4.76	-5.44	-5.87	-5.73
VY Car	2	52	7.71	7.3	5.1	-4.31	-5.04	-5.75	-6.17	-6.05
XY Car	0	67	7.83	6.3	4.4	-4.04	-4.76	-5.44	-5.87	-5.73
XZ Car	0	57	7.75	6.9	4.9	-4.14	-4.87	-5.57	-6.01	-5.87
YZ Car	3	55	7.74	6.9	4.9	-4.14	-4.87	-5.57	-6.01	-5.87
AQ Car	0	78	7.89	6.0	4.2	-3.89	-4.58	-5.24	-5.65	-5.52
HW Car	0	80	7.91	6.0	4.2	-3.89	-4.58	-5.24	-5.65	-5.52
SZ Cyg	3	62	7.8	6.6	4.6	-3.99	-4.71	-5.4	-5.83	-5.69
CD Cyg	3	58	7.76	6.9	4.9	-4.14	-4.87	-5.57	-6.01	-5.87
VX Per	2	69	7.84	6.3	4.4	-4.04	-4.76	-5.44	-5.87	-5.73
X Pup	3	44	7.64	7.8	5.4	-4.42	-5.15	-5.87	-6.29	-6.17
AQ Pup	3	40	7.6	8.2	5.7	-4.48	-5.24	-5.98	-6.41	-6.29
WZ Sgr	3	49	7.69	7.3	5.1	-4.31	-5.04	-5.75	-6.17	-6.05
RY Sco	3	52	7.71	7.3	5.1	-4.31	-5.04	-5.75	-6.17	-6.05
Z Sct	3	69	7.84	6.3	4.4	-4.04	-4.76	-5.44	-5.87	-5.73
S Vul	3	24	7.37	10.2	7.2	-4.55	-5.76	-7.1	-7.63	-7.6
DD Cas (B4V)	3	82	7.92	6.0	4.95	-3.21	-3.93	-4.62	-5.05	-4.92
KN Cen (B2V)	3	37	7.57	8.6	6.9	-3.75	-4.74	-5.77	-6.28	-6.18

NOTE—Column X marks the instability crossing based on positive (assumed to be third crossings) and negative (second crossings) observed period changes (Turner et al. 2006). Ages are estimated using period-age relations for the appropriate crossing assuming average initial rotation rates (Anderson et al. 2016a). Cepheid masses m_1 are estimated using isochrones of Solar metallicity and average ZAMS rotation (Ekström et al. 2012; Georgy et al. 2013) for a fixed adopted mean color $V - I = 0.5$ during the blue loop phase. m_2 is the mass of a hypothetical companion, where $m_2/m_1 = 0.7$ for most cases (see §5.2) for the purpose of estimating the contrast in different filters and filter combinations. DD Cas and KN Cen are marked together with companion spectral type estimates (Madore 1977). The Cepheids in this program are between 25 and 80 Myr old. Cepheids are much brighter than their main sequence companions, as expected, and this contrast increases when using longer-wavelength data and Wesenheit indices, as well as with pulsation period.

the typical contrast using Wesenheit formulations or H -band photometry is on the order of 6 magnitudes at the typical period ($\log P_{\text{puls}} \sim 1.3$) of extragalactic Cepheid samples (S. L. Hoffmann et al., submitted). The associated increase in brightness of -0.004 mag is much lower than the width of the instability strip (Riess et al. 2016, 0.08 mag in H -band) and would lead to a distance error of merely 0.2% for an individual star—much less for an entire population. Binaries with lower contrast—such as KN Cen and DD Cas—are expected to be the exception and even for these cases, no strong photometric bias is expected in H -band. Furthermore, selection criteria applied in the search for extragalactic Cepheids such as amplitude ratios are expected to remove very strong outliers (e.g. Hoffmann &

Macri 2015). While photometric bias is comparatively stronger for shorter-period Cepheids and in optical passbands, we conclude that the light contributed by typical companion stars is on average negligible for distance scale applications where large numbers Cepheids are observed using near infrared photometry and/or Wesenheit magnitudes.

An important additional consideration for the accuracy of parallax measurements is the phase-dependence of the contrast between a Cepheid and its spatially unresolved companion that shifts the measured photocenter in phase with the Cepheid’s variability. This effect has been referred to as “Variability Induced Movers” (Wielen 1996, VIM) in the context of *Hipparcos* (Perryman & ESA 1997; van Leeuwen 2007). Whereas most *Hippar-*

cos VIM solutions were later found to be color-induced (Pourbaix et al. 2003), the correction for VIM-type effects is an integral part of *Gaia* data processing (CU4) due to *Gaia*'s much increased astrometric precision. The same effect can also impact our *HST* spatial scanning measurements, depending on i) the orientation of the scan direction with respect to the orientation of the binary; ii) the (unresolved) angular separation of the two components; iii) the average contrast between Cepheid and companion in the passband used to measure parallax; iv) the pulsation phases sampled by the scan observations. We will study this effect in detail and constrain its impact on our Cepheid parallaxes in future work.

5.3. Peculiar variability

Cepheids with variability periods longer than ~ 20 d have been shown in the literature to exhibit non-linear variations of P_{puls} and other cycle-to-cycle modulations (e.g. Berdnikov et al. 2000; Anderson 2014). Among the present sample, the most affected stars are KN Cen, X Pup, AQ Pup, and S Vul, with AQ Pup having been discussed as a candidate for a first crossing Cepheid (Anderson et al. 2016a).

Nonlinear changes of P_{puls} complicate the inference of mean magnitudes from photometric measurements taken at random times using a known pulsation ephemeris. In the worst case, non-linear period changes may lead to a complete loss of knowledge of the pulsation phase, leading to observations observed at random phase. Near-IR photometry can partially mitigate the scatter of the PLR determined by random-phase observations, since pulsation amplitudes decrease with increasing wavelength. For a given galaxy, the distance error contribution by this term is < 0.12 mag, slightly larger than the intrinsic dispersion of the Leavitt law in the *H*-band (Riess et al. 2016).

At present, it is not clear what fraction of Cepheids exhibits such effects and how these phenomena are related to the ability to use affected Cepheids as precise standard candles. A characterization of non-linear period changes in extragalactic Cepheids has thus far only been possible in the Magellanic clouds (Poleski 2008; Soszyński et al. 2015, Süveges & Anderson, submitted). *Gaia* parallaxes and the ability to study Galactic Cepheids in great detail will enable a better understanding of pulsation irregularities and inform the vetting process of high-accuracy Leavitt law calibrators accordingly.

6. CONCLUSIONS

Over the course of 5 years, we have observed more than 1600 high-precision RVs of 19 Galactic classical long-period Cepheids for which the SH0ES team is measuring highly accurate trigonometric parallaxes using

HST/WFC3 spatial scans (Riess et al. 2014; Casertano et al. 2016).

We investigate the RV variability of all program Cepheids and construct the most detailed view of Fourier parameters R_{21} , R_{31} , ϕ_{21} , and ϕ_{31} as a function of pulsation period.

We determine upper limits for undetected spectroscopic companion stars with $P_{\text{orb}} \lesssim 5$ yr for 18 of the 19 program Cepheids assuming circular orbital motion for a range of input values of P_{orb} . For YZ Carinae, we determine a corrected, full Keplerian orbital solution with $P_{\text{orb}} \sim 830$ d (§4.2).

Using the upper limits on undetected spectroscopic binary configurations in combination with the properties of the actual *HST/WFC3* spatial scan observations, we compute the absolute inclination-projected maximal parallax error due to orbital motion, $\hat{w} \sin i$, that such “allowed” companions could introduce if the *HST* measurements are modeled assuming single star astrometric models. We quote the parallax error times $\sin i$ to underline that these limits are based on RV measurements, which cannot constrain inclination.

We exclude significant ($> 2\%$) parallax error due to orbital motion for the majority of Cepheids with *HST* measurements. We stress that the values of $\hat{w} \sin i$ quoted here are not indicative of a detected effect on the measured parallax, being entirely limited by the available data since no orbital motion was detected for 18 of the 19 Cepheids over the baseline of interest for the parallax measurements ($P_{\text{orb}} \lesssim 5$ yr).

We estimate that YZ Carinae’s parallax would be affected by approximately 30% ($\sim \pm 100 \mu\text{arcsec}$) if the astrometric measurements were modeled assuming a single star configuration. We will therefore obtain additional spatial scan epochs of this star to enable fitting for the orbit in the astrometric modeling.

We additionally investigate variations of the pulsation-averaged velocity v_γ to search for indications of possible long-timescale ($P_{\text{orb}} \gtrsim 10$ yr) binarity. We thus report

- the discovery of the spectroscopic binary nature of XZ Car and CD Cyg, as well as tentative evidence for AQ Car’s time-variable v_γ ;
- first evidence for orbital motion of KN Cen, which has a known B-star companion;
- a first clear indication of orbital motion for SSC Ma;
- evidence supporting the spectroscopic binarity of VY Car and X Pup, as well as tentative evidence for SZ Cyg;

- that AQ Pup and WZ Sgr are likely not to be spectroscopic binaries despite previous claims.

Since the associated orbital periods are much longer than the 5yr baseline of the *HST* spatial scanning observations, no parallax error due to orbital motion is expected for these stars. The binary fraction in our sample is 32–52%, cf. §5.1.

We further discuss the typical photometric impact of unresolved companions based on stellar isochrones. This leads to the conclusion that near-IR photometry and/or Wesenheit magnitudes are well-suited to reduce the photometric bias due to such companions (typical contrast of ~ 6 mag in *H*-band at $\log P_{\text{puls}} \sim 1.3$). Moreover, the contrast between a Cepheid and its typical main sequence companion increases with P_{puls} , i.e., longer-period Cepheids are on average less biased by flux contributed by unresolved companions. Near-IR photometry is furthermore well-suited to mitigate PLR scatter in the presence of non-linear fluctuations of P_{puls} thanks to lower IR amplitudes.

Galactic Cepheids present the unique opportunity to conduct a detailed vetting of candidates for which the most accurate calibration between pulsation period and average absolute magnitude can be achieved. In the era of high-accuracy parallax measurements of long-period Cepheids heralded by *Gaia* and the *HST/WFC3* spatial scan observations, such a vetting process may help to increase the accuracy of the extragalactic distance scale from the bottom up. Further work along the lines presented here will benefit the overarching goal of determining the value of the local Hubble constant H_0 to 1% accuracy and a better understanding of Dark Energy.

We acknowledge observational assistance by Pierre Dubath, Marion Neveu, Janis Hagelberg, Dominique Naef, Nicolas Cantale, and Malte Tewes. We thank all

Euler and Mercator support staff for their competent assistance. We further thank the referee for a timely and constructive report.

We thank Laszlo Szabados for maintaining the openly accessible database of Cepheid binaries⁷. This resource was an invaluable help to track down relevant literature for this research. We further made use of the DDO Cepheids database⁸ (Fernie et al. 1995) and the McMaster Cepheid photometry and RV data archive⁹ maintained by Doug Welch. We thank Christiaan Sterken for communicating RV data by Caldwell et al. (2001).

This research is based on observations made with the Mercator Telescope, operated on the island of La Palma by the Flemish Community, at the Spanish Observatorio del Roque de los Muchachos of the Instituto de Astrofísica de Canarias. *HERMES* supported by the Fund for Scientific Research of Flanders (FWO), Belgium, the Research Council of K.U. Leuven, Belgium, the Fonds National de la Recherche Scientifique (F.R.S.-FNRS), Belgium, the Royal Observatory of Belgium, the Observatoire de Genève, Switzerland, and the Thüringer Landessternwarte, Tautenburg, Germany.

This research has made use of NASA’s ADS Bibliographic Services; the SIMBAD database and the VizieR catalogue access tool¹⁰ provided by CDS, Strasbourg; Astropy, a community-developed core Python package for Astronomy (Astropy Collaboration et al. 2013); the International Variable Star Index (VSX) database, operated at AAVSO, Cambridge, Massachusetts, USA.

RIA acknowledges funding from the Swiss National Science Foundation through an Early Postdoc.Mobility fellowship. CM acknowledges support from the US National Science Foundation through award NSF-AST-1313428. PIP is a Postdoctoral Fellow of the The Research Foundation – Flanders (FWO), Belgium. This research was supported by the Munich Institute for Astro and Particle Physics (MIAPP) of the DFG cluster of excellence ”Origin and Structure of the Universe”.

REFERENCES

- Aikawa, T., & Antonello, E. 2000, *A&A*, 363, 593
 Anderson, R. I. 2013, PhD thesis, Université de Genève
 —. 2014, *A&A*, 566, L10
 Anderson, R. I., Eyer, L., & Mowlavi, N. 2013, *MNRAS*, 434, 2238
 Anderson, R. I., Sahlmann, J., Holl, B., et al. 2015, *ApJ*, 804, 144
 Anderson, R. I., Saio, H., Ekström, S., Georgy, C., & Meynet, G. 2016a, *A&A*, 591, A8
- ⁷ <http://www.konkoly.hu/CEP/intro.html>
⁸ <http://www.astro.utoronto.ca/DDO/research/Cepheids/>
⁹ <http://crocus.physics.mcmaster.ca/Cepheid/>
¹⁰ <http://cdsweb.u-strasbg.fr/>
- Anderson, R. I., Mérand, A., Kervella, P., et al. 2016b, *MNRAS*, 455, 4231
 Antonello, E., & Morelli, P. L. 1996, *A&A*, 314, 541
 Astropy Collaboration, Robitaille, T. P., Tollerud, E. J., et al. 2013, *A&A*, 558, A33
 Baade, W. 1944, *ApJ*, 100, 137
 —. 1956, *PASP*, 68, 5
 Baranne, A., Queloz, D., Mayor, M., et al. 1996, *A&AS*, 119, 373
 Barnes, III, T. G., Moffett, T. J., & Slovak, M. H. 1988, *ApJS*, 66, 43
 Benedict, G. F., McArthur, B. E., Fredrick, L. W., et al. 2002, *AJ*, 124, 1695
 Benedict, G. F., McArthur, B. E., Feast, M. W., et al. 2007, *AJ*, 133, 1810
 Berdnikov, L. N., Henden, A. A., Turner, D. G., & Pastukhova, E. N. 2009, *Astronomy Letters*, 35, 406

- Berdnikov, L. N., & Ignatova, V. V. 2000, in *Astronomical Society of the Pacific Conference Series*, Vol. 203, IAU Colloq. 176: The Impact of Large-Scale Surveys on Pulsating Star Research, ed. L. Szabados & D. Kurtz, 244–245
- Berdnikov, L. N., Ignatova, V. V., Caldwell, J. A. R., & Koen, C. 2000, *NewA*, 4, 625
- Bersier, D. 2002, *ApJS*, 140, 465
- Bhardwaj, A., Kanbur, S. M., Macri, L. M., et al. 2016, *MNRAS*, 457, 1644
- Böhm-Vitense, E., & Proffitt, C. 1985, *ApJ*, 296, 175
- Caldwell, J. A. R., Coulson, I. M., Dean, J. F., & Berdnikov, L. N. 2001, *Journal of Astronomical Data*, 7
- Casertano, S., Riess, A. G., Anderson, J., et al. 2016, *ApJ*, 825, 11
- Coulson, I. M. 1983, *MNRAS*, 205, 1135
- Coulson, I. M., & Caldwell, J. A. R. 1985, *South African Astronomical Observatory Circular*, 9, 5
- Coulson, I. M., Caldwell, J. A. R., & Gieren, W. P. 1985, *ApJS*, 57, 595
- de Bruijne, J. H. J., & Eilers, A.-C. 2012, *A&A*, 546, A61
- Derekas, A., Szabó, G. M., Berdnikov, L., et al. 2012, *MNRAS*, 425, 1312
- Ekström, S., Georgy, C., Eggenberger, P., et al. 2012, *A&A*, 537, A146
- Evans, N. R. 1994, *ApJ*, 436, 273
- . 1995, *ApJ*, 445, 393
- Evans, N. R., Bond, H. E., Schaefer, G. H., et al. 2013, *AJ*, 146, 93
- . 2016a, *AJ*, 151, 129
- Evans, N. R., & Udalski, A. 1994, *AJ*, 108, 653
- Evans, N. R., Berdnikov, L., Lauer, J., et al. 2015, *AJ*, 150, 13
- Evans, N. R., Pillitteri, I., Wolk, S., et al. 2016b, *AJ*, 151, 108
- Eyer, L., Palaversa, L., Mowlavi, N., et al. 2012, *Ap&SS*, 341, 207
- Feast, M. W., & Catchpole, R. M. 1997, *MNRAS*, 286, L1
- Fernie, J. D., Evans, N. R., Beattie, B., & Seager, S. 1995, *Information Bulletin on Variable Stars*, 4148, 1
- Fernie, J. D., Hiltner, W. A., & Kraft, R. P. 1966, *AJ*, 71, 999
- Freedman, W. L., Madore, B. F., Gibson, B. K., et al. 2001, *ApJ*, 553, 47
- Gallenne, A., Mérand, A., Kervella, P., et al. 2015, *A&A*, 579, A68
- Gallenne, A., Merand, A., Kervella, P., et al. 2016, *ArXiv e-prints*, arXiv:1606.01108
- García-Varela, A., Muñoz, J. R., Sabogal, B. E., Vargas Domínguez, S., & Martínez, J. 2016, *ApJ*, 824, 74
- Georgy, C., Ekström, S., Granada, A., et al. 2013, *A&A*, 553, A24
- Gorynya, N. A., Irsamambetova, T. R., Rastorgouev, A. S., & Samus, N. N. 1992, *Soviet Astronomy Letters*, 18, 316
- Hertzprung, E. 1913, *Astronomische Nachrichten*, 196, 201
- Hilditch, R. W. 2001, *An Introduction to Close Binary Stars (CUP)*
- Hoffmann, S. L., & Macri, L. M. 2015, *AJ*, 149, 183
- Imbert, M. 1999, *A&AS*, 140, 79
- Inno, L., Matsunaga, N., Bono, G., et al. 2013, *ApJ*, 764, 84
- Joy, A. H. 1937, *ApJ*, 86, 363
- Kanbur, S. M., Marconi, M., Ngeow, C., et al. 2010, *MNRAS*, 408, 695
- Kovacs, G., Kisvarsanyi, E. G., & Buchler, J. R. 1990, *ApJ*, 351, 606
- Kurochkin, N. E. 1966, *Peremennye Zvezdy*, 16, 10
- Leavitt, H. S., & Pickering, E. C. 1912, *Harvard College Observatory Circular*, 173, 1
- Lloyd Evans, T. 1968, *MNRAS*, 141, 109
- . 1980, *South African Astronomical Observatory Circular*, 1, 257
- Madore, B. F. 1977, *MNRAS*, 178, 505
- . 1982, *ApJ*, 253, 575
- Madore, B. F., & Fernie, J. D. 1980, *PASP*, 92, 315
- Mahmoud, F., & Szabados, L. 1980, *Information Bulletin on Variable Stars*, 1895
- Makarenko, E. N. 1978, *Astronomicheskij Tsirkulyar*, 1003, 4
- Michalik, D., Lindegren, L., & Hobbs, D. 2015, *A&A*, 574, A115
- Neilson, H. R., Schneider, F. R. N., Izzard, R. G., Evans, N. R., & Langer, N. 2015, *A&A*, 574, A2
- Pakhomov, Y. V., & Zhao, G. 2013, *AJ*, 146, 97
- Pel, J. W. 1978, *A&A*, 62, 75
- Pepe, F., Mayor, M., Galland, F., et al. 2002, *A&A*, 388, 632
- Perryman, M. A. C., & ESA, eds. 1997, *ESA Special Publication*, Vol. 1200, *The HIPPARCOS and TYCHO catalogues. Astrometric and photometric star catalogues derived from the ESA HIPPARCOS Space Astrometry Mission*
- Petterson, O. K. L., Cottrell, P. L., & Albrow, M. D. 2004, *MNRAS*, 350, 95
- Petterson, O. K. L., Cottrell, P. L., Albrow, M. D., & Fokin, A. 2005, *MNRAS*, 362, 1167
- Pojmanski, G. 2002, *Acta Astron.*, 52, 397
- Poleski, R. 2008, *Acta Astron.*, 58, 313
- Pont, F., Burki, G., & Mayor, M. 1994, *A&AS*, 105, 165
- Pourbaix, D., Platais, I., Detournay, S., et al. 2003, *A&A*, 399, 1167
- Proust, D., Ochsenbein, F., & Pettersen, B. R. 1981, *A&AS*, 44, 179
- Riess, A. G., Casertano, S., Anderson, J., MacKenty, J., & Filippenko, A. V. 2014, *ApJ*, 785, 161
- Riess, A. G., Macri, L., Casertano, S., et al. 2009, *ApJ*, 699, 539
- . 2011, *ApJ*, 730, 119
- Riess, A. G., Macri, L. M., Hoffmann, S. L., et al. 2016, *ArXiv e-prints*, arXiv:1604.01424
- Samus, N. N., Durlevich, O. V., & et al. 2009, *VizieR Online Data Catalog*, 1, 2025
- Sandage, A., Tammann, G. A., & Reindl, B. 2009, *A&A*, 493, 471
- Simon, N. R., & Lee, A. S. 1981, *ApJ*, 248, 291
- Soszyński, I., Poleski, R., Udalski, A., et al. 2008, *Acta Astron.*, 58, 163
- Soszyński, I., Udalski, A., Szymański, M. K., et al. 2015, *Acta Astron.*, 65, 329
- Stibbs, D. W. N. 1955, *MNRAS*, 115, 363
- Stobie, R. S. 1970, *MNRAS*, 148, 1
- Storm, J., Gieren, W., Fouqué, P., et al. 2011, *A&A*, 534, A94
- Struve, O. 1945, *ApJ*, 102, 232
- Suyu, S. H., Treu, T., Blandford, R. D., et al. 2012, *ArXiv e-prints*, arXiv:1202.4459
- Szabados, L. 1989, *Communications of the Konkoly Observatory Hungary*, 94
- . 1991, *Communications of the Konkoly Observatory Hungary*, 96, 123
- . 1996, *A&A*, 311, 189
- . 2003, *IBVS*, 5394, 1
- Szabados, L., Derekas, A., Kiss, C., & Klagyivik, P. 2012, *MNRAS*, 426, 3154
- Turner, D. G. 1977, *AJ*, 82, 163
- Turner, D. G., Abdel-Sabour Abdel-Latif, M., & Berdnikov, L. N. 2006, *PASP*, 118, 410
- Turner, D. G., van den Bergh, S., Younger, P. F., Danks, T. A., & Forbes, D. 1993, *ApJS*, 85, 119
- Turner, D. G., van den Bergh, S., Younger, P. F., et al. 2012, *AJ*, 144, 187
- van Leeuwen, F., ed. 2007, *Astrophysics and Space Science Library*, Vol. 350, *Hipparcos, the New Reduction of the Raw Data*
- van Leeuwen, F., Feast, M. W., Whitelock, P. A., & Laney, C. D. 2007, *MNRAS*, 379, 723
- Vinko, J. 1991, *Ap&SS*, 183, 17

Wallerstein, G., Jacobsen, T. S., Cottrell, P. L., Clark, M., & Albrow, M. 1992, MNRAS, 259, 474

Walraven, J. H., Tinbergen, J., & Walraven, T. 1964, Bull. Astron. Inst. Netherlands, 17, 520

Facilities:

Facility: Mercator1.2m,

Weinberg, D. H., Mortonson, M. J., Eisenstein, D. J., et al. 2013, Phys. Rep., 530, 87

Wielen, R. 1996, A&A, 314

Facility: Shane3m,

Facility: Euler1.2m